eLIFE – Research Article

Presynaptic NMDA receptors facilitate short-term plasticity and BDNF release at hippocampal mossy fiber synapses

Pablo J. Lituma[1], Hyung-Bae Kwon[1,4], Rafael Lujan[3], Pablo E. Castillo[1,2]*

[1] Dominick P. Purpura Department of Neuroscience, Albert Einstein College of Medicine, Bronx, NY 10461, U.S.A.
[2] Department of Psychiatry and Behavioral Sciences, Albert Einstein College of Medicine, Bronx, NY 10461, U.S.A.
[3] Instituto de Investigación en Discapacidades Neurológicas (IDINE), Facultad de Medicina, Universidad Castilla-La Mancha, 02008 Albacete, Spain.
[4] Present address: The Solomon H. Snyder Department of Neuroscience, John Hopkins University, School of Medicine, Baltimore, MD 21205

Running title: Role of presynaptic NMDA receptors in short-term plasticity

Keywords: CA3, ionotropic, hippocampus, presynaptic calcium, autoreceptors

* To whom correspondence should be addressed:

Pablo E. Castillo, MD/PhD
Dominick P. Purpura Department of Neuroscience
Albert Einstein College of Medicine
1410 Pelham Parkway South
Kennedy Center, Room 703
Bronx, NY 10461, USA
Email: pablo.castillo@einsteinmed.org

Title: 99 characters (with spaces)
Abstract: 139 words, 1081 characters with spaces
Main text (excluding Summary, Methods, references and figure legends): 4,369
Figures: 8
Supplemental figures: 6

Abstract

Neurotransmitter release is a highly controlled process by which synapses can critically regulate information transfer within neural circuits. While presynaptic receptors –typically activated by neurotransmitters and modulated by neuromodulators– provide a powerful way of fine tuning synaptic function, their contribution to activity-dependent changes in transmitter release remains poorly understood. Here, we report that presynaptic NMDA receptors (preNMDARs) at hippocampal mossy fiber boutons can be activated by physiologically relevant patterns of activity and selectively enhance short-term synaptic plasticity at mossy fiber inputs onto CA3 pyramidal cells and mossy cells, but not onto inhibitory interneurons. Moreover, preNMDARs facilitate brain-derived neurotrophic factor (BDNF) release and contribute to presynaptic calcium rise. Taken together, our results indicate that preNMDARs, by increasing presynaptic calcium, fine tune mossy fiber neurotransmission and can control information transfer during dentate granule cell burst activity that normally occur *in vivo*.

Introduction

Neurotransmission is a dynamic and highly regulated process. The activation of ionotropic and metabotropic presynaptic receptors provides a powerful way of fine tuning neurotransmission via the facilitation or inhibition of neurotransmitter release (Burke & Bender, 2019; Engelman & MacDermott, 2004; Miller, 1998; Pinheiro & Mulle, 2008; Schicker, Dorostkar, & Boehm, 2008). Due to their unique functional properties, including high calcium-permeability, slow kinetics and well-characterized role as coincidence-detectors (Cull-Candy, Brickley, & Farrant, 2001; Lau & Zukin, 2007; Paoletti, Bellone, & Zhou, 2013; Traynelis et al., 2010), presynaptic NMDA receptors (preNMDARs) have emerged as key regulators of synaptic transmission and plasticity (Banerjee, Larsen, Philpot, & Paulsen, 2016; Bouvier, Bidoret, Casado, & Paoletti, 2015; Bouvier, Larsen, Rodriguez-Moreno, Paulsen, & Sjostrom, 2018; Duguid, 2013; Duguid & Smart, 2009; Wong, Rannio, Jones, Thomazeau, & Sjostrom, 2020). Regulation of neurotransmitter release by NMDA autoreceptors in the brain was suggested three decades ago (Martin, Bustos, Bowe, Bray, & Nadler, 1991). Anatomical evidence for preNMDARs arose from an immuno-electron microscopy study revealing NMDARs at the mossy fiber giant bouton of the monkey hippocampus (Siegel et al., 1994), followed by functional studies in the entorhinal cortex indicating that preNMDARs tonically increase spontaneous glutamate release and also facilitate evoked release in a frequency-dependent manner (Berretta & Jones, 1996; Woodhall, Evans, Cunningham, & Jones, 2001). Since these early studies, although evidence for preNMDARs has accumulated throughout the brain (Banerjee et al., 2016; Bouvier et al., 2018; Duguid & Smart, 2009), the presence and functional relevance of preNMDARs at key synapses in the brain have been called into question (Carter & Jahr, 2016; Duguid, 2013).

Mossy fibers – the axons of dentate granule cells (GCs) – establish excitatory synapses onto

proximal dendrites of CA3 pyramidal neurons, thereby conveying a major excitatory input to the hippocampus proper (Amaral, Scharfman, & Lavenex, 2007; Henze, Urban, & Barrionuevo, 2000). This synapse displays uniquely robust frequency facilitation both *in vitro* (Nicoll & Schmitz, 2005; Salin, Scanziani, Malenka, & Nicoll, 1996; Vyleta, Borges-Merjane, & Jonas, 2016) and *in vivo* (Hagena & Manahan-Vaughan, 2010; Vandael, Borges-Merjane, Zhang, & Jonas, 2020). The molecular basis of this short-term plasticity is not fully understood but likely relies on diverse presynaptic mechanisms that increase glutamate release (Jackman & Regehr, 2017; Rebola, Carta, & Mulle, 2017). Short-term, use-dependent facilitation is believed to play a critical role in information transfer, circuit dynamics and short-term memory (Abbott & Regehr, 2004; Jackman & Regehr, 2017; Klug et al., 2012). The mf-CA3 synapse can strongly drive the CA3 network during short bursts of presynaptic activity (Chamberland, Timofeeva, Evstratova, Volynski, & Toth, 2018; Henze, Wittner, & Buzsaki, 2002; Vyleta et al., 2016; Zucca et al., 2017), an effect that likely results from two key properties of this synapse, namely, its strong frequency facilitation and proximal dendritic localization. In addition to CA3 pyramidal neurons, mossy fiber axons establish synaptic connections with hilar mossy cells (MC) and inhibitory interneurons (IN) (Amaral et al., 2007; Henze et al., 2000). These connections also display robust short-term plasticity (Lysetskiy, Foldy, & Soltesz, 2005; Toth, Suares, Lawrence, Philips-Tansey, & McBain, 2000), which may contribute significantly to information transfer and dynamic modulation of the dentate gyrus (DG)-CA3 circuit (Bischofberger, Engel, Frotscher, & Jonas, 2006; Evstratova & Toth, 2014; Lawrence & McBain, 2003). Despite early evidence for preNMDARs at mossy fiber boutons (Siegel et al., 1994), whether these receptors modulate neurotransmission at mossy fiber synapses is unknown. Intriguingly, mossy fibers contain one of the highest expression levels of brain-derived neurotrophic factor, BDNF (Conner, Lauterborn, Yan, Gall, & Varon, 1997). While preNMDARs were implicated in BDNF release at corticostriatal synapses (Park, Popescu, & Poo, 2014), whether putative preNMDARs impact BDNF release at mossy fiber synapses remains unexplored.

Here, to examine the potential presence and impact of preNMDARs at mossy fiber synapses, we utilized multiple approaches, including immunoelectron microscopy, selective pharmacology for NMDARs, a genetic knockout strategy to remove NMDARs from presynaptic GCs, two-photon imaging of BDNF release, and presynaptic calcium signals in acute rodent hippocampal slices. Our findings indicate that preNMDARs, likely by increasing presynaptic calcium, contribute to mossy fiber short-term plasticity and promotes BDNF release. Thus, preNMDARs at mossy fibers may facilitate information transfer and provide an important point of regulation in the DG – CA3 circuit by fine-tuning both glutamate and BDNF release.

Results

Electron microscopy reveals presynaptic NMDA receptors at mossy fiber terminals

To determine the potential localization of NMDA receptors at the mossy fiber terminals of the rodent hippocampus, we performed electron microscopy and post-embedding immunogold labeling in rats using a validated antibody for the obligatory subunit GluN1 (Petralia, Yokotani, & Wenthold, 1994; Siegel et al., 1994; Takumi, Ramirez-Leon, Laake, Rinvik, & Ottersen, 1999; Watanabe et al., 1998). Gold particles were detected in the main body of the postsynaptic density as well as presynaptic mossy fiber terminals (**Figure 1A-C**). GluN1 localized in mossy fiber boutons in a relatively high proportion to the active zone, as compared to associational-commissural (ac) synapse in the same CA3 pyramidal neuron (**Figure 1D**; mf, ~32% presynaptic particles; ac, <10% presynaptic particles; n = 3 animals). Similar quantification for AMPA receptors did not reveal presynaptic localization of these receptors in either mossy fiber or associational commissural synapses (**Figure S1A-C**; ~5% presynaptic particles, n = 3 animals). Together, these results provide anatomical evidence for preNMDARs at mf-CA3 synapses.

Both NMDAR antagonism and genetic deletion from presynaptic granule cells reduce mossy fiber low-frequency facilitation

Presynaptic short-term plasticity, in the form of low-frequency (~1 Hz) facilitation (LFF), is uniquely robust at the mf-CA3 synapse (Nicoll & Schmitz, 2005; Salin et al., 1996). To test a potential involvement of preNMDARs in LFF, we monitored CA3 pyramidal neurons in acute rat hippocampal slices. Neurons were held at Vh= -70 mV to minimize postsynaptic NMDAR conductance, and mossy fibers were focally stimulated with a bipolar electrode (theta glass pipette) in *stratum lucidum* ~100 µm from the recorded cell. LFF of AMPAR-mediated transmission was induced by stepping the stimulation frequency from 0.1 Hz to 1 Hz for ~2 min in the presence of picrotoxin (100 µM) to block fast inhibitory synaptic transmission, and a low concentration of the AMPAR noncompetitive antagonist LY303070 (0.5 µM) to minimize CA3-CA3 recurrent activity (Kwon & Castillo, 2008). Bath-application of the NMDAR irreversible open channel blocker MK-801 (50 µM) significantly reduced LFF (**Figure 1E**). In addition, the competitive NMDAR antagonists D-APV (100 µM) or R-CPP (50 µM) yielded a comparable reduction of facilitation (**Figure 1F**). To confirm that these synaptic responses were mediated by mossy fibers, the mGluR2/3 agonist DCG-IV (1 µM) was applied at the end of all recordings (Kamiya, Shinozaki, & Yamamoto, 1996). To control for stability, we performed interleaved experiments in the absence of NMDAR antagonists and found that LFF remained unchanged (**Figure S2A**). These findings indicate NMDAR antagonism reduces mf-CA3 short-term plasticity (LFF), suggesting that preNMDARs could contribute to this form of presynaptic plasticity.

The reduction in facilitation of AMPAR-transmission could be due to dampening of CA3 recurrent activity by NMDAR antagonism (Henze et al., 2000; Kwon & Castillo, 2008; Nicoll & Schmitz, 2005). To discard this possibility, we repeated our experiments in a much less excitable network in which AMPAR-mediated synaptic transmission was selectively blocked by a high concentration of the noncompetitive antagonist LY303070 (15 µM), and monitored the kainate receptor (KAR)-

mediated component of mossy fiber synaptic transmission (Castillo, Malenka, & Nicoll, 1997; Kwon & Castillo, 2008). In addition, 2 mM MK-801 was included in the intracellular recording solution to block postsynaptic NMDARs (Corlew, Brasier, Feldman, & Philpot, 2008) (**Figure S3A**). To further ensure postsynaptic NMDAR blockade, we voltage-clamped the CA3 pyramidal neuron at -70 mV and waited until NMDAR-mediated transmission was eliminated and only KAR-EPSCs remained. Under these recording conditions, bath-application of MK-801 (50 μM) also reduced LFF of KAR-mediated transmission (**Figure 1G**), whereas LFF remained unchanged in interleaved control experiments (**Figure S2B**). At the end of these recordings**,** 10 μM NBQX was applied to confirm KAR-transmission (**Figure 1G; Figure S2B**) (Castillo et al., 1997; Kwon & Castillo, 2008). It is therefore unlikely that the reduction of LFF mediated by NMDAR antagonism could be explained by recurrent network activity, suggesting a direct effect on transmitter release.

To further support a role of preNMDARs in mossy fiber LFF, we took a genetic approach by conditionally removing NMDARs from GCs in *Grin1* floxed mice. To this end, an AAV5-CamKII-Cre-GFP virus was bilaterally injected in the DG to selectively delete *Grin1* expression, whereas AAV5-CamKII-eGFP was injected in littermates as a control (**Figure 2A**). Two weeks after surgery, we prepared acute hippocampal slices and examined the efficacy of *Grin1* deletion by analyzing NMDAR-mediated transmission in GFP^+ GCs of *Grin1*-cKO and control mice. We confirmed that in contrast to control mice, no NMDAR-EPSCs were elicited by electrically stimulating medial perforant path inputs in *Grin1*-cKO GCs voltage-clamped at +40 mV in the presence of 100 μM picrotoxin and 10 μM NBQX (**Figure 2B**). As expected, the NMDAR/AMPAR ratio was significantly reduced in *Grin1*-cKO mice compared to control (**Figure 2C**). Only acute slices that exhibited robust GFP fluorescence in the DG were tested for LFF of AMPAR-transmission in CA3. We found that LFF was significantly reduced in *Grin1*-cKOs as compared to controls (**Figure 2D**), indicating that genetic removal of NMDARs from GCs recapitulated NMDAR antagonism (**Figure 1E-G**). *Grin1* deletion did not affect basal transmitter release as indicated by the lack of change

in paired-pulse ratio (Control: 2.5 ± 0.36, n = 13 cells; *Grin1* cKO: 2.4 ± 0.31, n = 13 cells; U = 0.758, Mann-Whitney test). Collectively, our findings using two distinct approaches strongly suggest that NMDAR activation in GCs increases LFF of mf-CA3 synaptic transmission.

Reduced facilitation by NMDAR antagonism is independent of the granule cell somatodendritic compartment

Bath application of MK-801 could have blocked dendritic NMDARs in GCs and potentially affected transmitter release (Christie & Jahr, 2008; Duguid, 2013). To address this possibility, we repeated our experiments after performing a surgical cut in the granular layer of the DG in order to isolate mossy fiber axons from GCs (**Figure S4A**). Under these conditions, MK-801 bath application still reduced LFF (**Figure 3A**), and LFF was stable in control, acutely transected axons (**Figure 3B**). In addition, puffing D-APV (2 mM) in *stratum lucidum* near (~200 µm) the recorded neuron also reduced LFF (**Figure 3C**), whereas puffing ACSF had no effect (**Figure 3D**). Lastly, in a set of control experiments we confirmed that D-APV puffs were sufficient to transiently block NMDAR-mediated transmission in CA3 but not in DG (**Figure S4B,C**). Together, these results support the notion that LFF reduction was due to the blockade of preNMDARs but not somatodendritic NMDARs on GCs.

PreNMDARs impact burst-induced facilitation and information transfer

GCs *in vivo* typically fire in brief bursts (Diamantaki, Frey, Berens, Preston-Ferrer, & Burgalossi, 2016; GoodSmith et al., 2017; Henze et al., 2002; Pernia-Andrade & Jonas, 2014; Senzai & Buzsaki, 2017). To test whether preNMDARs contribute to synaptic facilitation that occurs during more physiological patterns of activity, mossy fibers were activated with brief bursts (5 stimuli, 25 Hz). We first took an optogenetic approach and used a Cre-dependent ChiEF virus to selectively light-activate mf-CA3 synapses in *Grin1*-cKO and control mice. Thus, animals were injected with a mix of AAV5-CamKII-CreGFP + AAV-DJ-FLEX-ChiEF-tdTomato viruses in the DG (**Figure 4A**).

At least four weeks after surgery, acute slices were prepared and burst-induced facilitation of AMPAR-mediated transmission in CA3 was assessed (**Figure 4B,C**). Burst-induced facilitation triggered by light activation and measured as the ratio of EPSCs elicited by the 5th and 1st pulse (P5/P1 ratio), was significantly reduced in *Grin1*-cKO animals as compared to controls. Because these bursts of activity can activate the CA3 network (Henze et al., 2000; Kwon & Castillo, 2008; Nicoll & Schmitz, 2005), we next monitored KAR-EPSCs under conditions of low excitability (as in Figure 1G). MK-801 bath application also reduced burst-induced facilitation, whereas facilitation remained unchanged in naïve slices (**Figure 4D,E**). Lastly, we tested whether preNMDARs, by facilitating glutamate release during bursting activity, could bring CA3 pyramidal neurons to threshold and trigger postsynaptic action potentials. To test this possibility, we monitored action potentials elicited by KAR-EPSPs (resting membrane potential -70 ± 2 mV) from CA3 pyramidal neurons intracellularly loaded with 2 mM MK-801. Under these recording conditions, MK-801 bath application significantly reduced the mean number of spikes per burst (**Figure 4F**). No changes in mean spikes per burst were observed in naïve slices over time (**Figure 4G**). Application of 10 µM NBQX at the end of these experiments confirmed that action potentials were induced by KAR-mediated synaptic responses. In control experiments we found that intracellular MK-801 effectively blocked postsynaptic NMDAR transmission during burst stimulation (**Figure S3B**). Altogether, these results indicate that preNMDARs at mf-CA3 synapses can contribute to information transfer from the DG to CA3.

PreNMDARs contribute to presynaptic calcium rise and can be activated by glutamate

PreNMDARs could facilitate glutamate and BDNF release by increasing presynaptic Ca^{2+} rise (Bouvier et al., 2016; Buchanan et al., 2012; Carter & Jahr, 2016; Corlew et al., 2008; Park et al., 2014). To test this possibility at mf-CA3 synapses we combined a conditional knockout strategy with calcium imaging using two-photon microscopy. We deleted preNMDARs by injecting AAV5-

CamKII-mCherry-Cre virus in the DG of *Grin1* floxed mice, and littermate animals injected with AAV5-CamKII-mCherry virus served as control (**Figure 5A**). Two weeks after surgery, we confirmed the efficacy of *Grin1* deletion by activating medial perforant path inputs and monitoring NMDAR/AMPAR ratios in GCs of control and *Grin1*-cKO animals (**Figure 5A**). Virtually no NMDAR-EPSCs were detected at Vh= +40 mV in *Grin1*-cKO animals (**Figure 5A**). Acute slices that exhibited robust mCherry fluorescence in the DG were taken for calcium imaging experiments. To maximize our ability to detect preNMDAR-mediated calcium signals, we used a recording solution that contained nominal Mg^{2+}, 4 mM Ca^{2+} and 10 µM D-Serine (Carter & Jahr, 2016). GCs expressing mCherry were patch-loaded with 35 µM Alexa 594 and 200 µM Fluo-5F, and mossy fiber axons were imaged and followed towards CA3 until giant boutons (white arrows) were identified (**Figure 5B**). We found that calcium transients (CaTs) elicited by direct current injection in the GC soma (5 action potentials, 25 Hz) were significantly smaller in *Grin1*-cKO animals as compared to control (**Figure 5C-E**). Thus, preNMDARs contribute significantly to presynaptic Ca^{2+} rise in mossy fiber boutons, and by this means facilitate synaptic transmission.

Lastly, we sought to determine if direct activation of preNMDARs could drive Ca^{2+} influx in mossy fiber giant boutons. To test this possibility, we elicited CaTs by two-photon uncaging (2PU) of glutamate on mossy fiber boutons of control and *Grin1*-cKO animals (**Figure 6A**). As previously described mCherry GCs were patch-loaded with Alexa 594 and Fluo-5F in a recording solution designed to maximize the detection of preNMDAR-mediated calcium signals (as in Figure 5). We first verified that glutamate 2PU-induced CaTs in dendritic spine heads of GCs were strongly reduced in *Grin1*-cKO animals as compared to controls (**Figure 6B,C**). To verify that reduced ΔG/R signals were a result of *Grin1* deletion and not differences in uncaging laser power, we performed a laser power intensity–response curve, and found that *Grin1*-cKO animals exhibited reduced ΔG/R signals as compared to control regardless of laser power intensity (**Figure S5**). We next measured glutamate 2PU-induced CaTs in mossy fiber giant boutons (identified as in

Figure 5B) and found that single uncaging pulses were insufficient to drive detectable CaTs in control boutons (**Figure S6**). However, a burst of 2PU stimulation (5 pulses, 25 Hz) induced CaTs in mossy fiber boutons of control but not in *Grin1*-cKO animals (**Figure 6D,E**). These findings indicate that brief bursts of glutamate 2PU, a manipulation that mimics endogenous release of glutamate during physiological patterns of activity, induces presynaptic Ca^{2+} influx in mossy fiber boutons by activating preNMDARs.

PreNMDARs promote BDNF release from mossy fiber boutons

Previous work implicated preNMDARs in the release of BDNF at corticostriatal synapses following repetitive activity and presynaptic calcium elevations (Park et al., 2014). Given the uniquely high expression levels of BDNF in mossy fibers (Conner et al., 1997; Yan et al., 1997), we examined the potential role for preNMDARs in BDNF release from mossy fiber terminals. To this end, a Cre-dependent BDNF reporter (BDNF-pHluorin) was injected in *Grin1*-floxed and control animals. Littermate mice were injected with a mix of AAV5-CamKII-mCherry-Cre + AAV-DJ-DIO-BDNF-pHluorin viruses in the DG (**Figure 7A**). At least four weeks after surgery, acute slices were prepared for two-photon microscopy to image mossy fiber boutons. After acquiring a stable baseline of BDNF-pHluorin signals, mossy fibers were repetitively activated (see Methods) (**Figure 7B**). BDNF-pHluorin signals were analyzed by measuring ΔF/F, where ΔF/F reductions indicate BDNF release (Park et al., 2014). We found that GluN1-deficient mossy fiber boutons showed a significant (~50%) reduction of BDNF release as compared to control (**Figure 7C-D**), suggesting preNMDARs contribute significantly to BDNF release during repetitive activity of mossy fiber synapses.

PreNMDAR-mediated regulation of mossy fiber synapses is input-specific

In addition to providing a major excitatory input to the hippocampus proper, mossy fiber axons also synapse onto excitatory hilar mossy cells and inhibitory neurons in CA3 (Amaral et al., 2007;

Henze et al., 2000; Lawrence & McBain, 2003). To test whether preNMDARs could also play a role at these synapses, we visually patched mossy cells and interneurons, loaded them with 35 µM Alexa 594 (**Figure 8A**) and 2 mM MK-801, and monitored AMPAR-EPSCs (Vh = -70 mV). Unlike mf-CA3 synapses, mossy fiber synapses onto CA3 interneurons in *stratum lucidum* do not express LFF, but can undergo burst-induced facilitation or depression (Toth et al., 2000). We found that MK-801 bath application had no significant effect on burst-induced facilitation or depression (**Figure 8B**), suggesting preNMDARs do not play a role at mf-Interneuron synapses in CA3. Mossy fiber inputs onto hilar mossy cells undergo robust activity-dependent facilitation (Lysetskiy et al., 2005). Like for mf-CA3 synapses, we found that MK-801 reduced LFF (**Figure 8C**). These findings strongly suggest that preNMDARs facilitate mossy fiber transmission onto excitatory neurons but not onto inhibitory interneurons.

Discussion

In this study, we provide evidence that hippocampal mossy fiber boutons express preNMDARs whose activation fine-tunes mossy fiber synaptic function. Specifically, our results show that preNMDARs enhance mossy fiber short-term plasticity in a target cell-specific manner. By enhancing glutamate release onto excitatory but not inhibitory interneurons, preNMDARs increase GC-CA3 spike transfer. Moreover, using two-photon calcium imaging, we demonstrate that preNMDARs contribute to presynaptic Ca^{2+} rise in mossy fiber boutons. Lastly, upon repetitive activity preNMDARs promote BDNF release from mossy fiber boutons. Taken together, our findings indicate that preNMDARs act as autoreceptors to boost both glutamate and BDNF release at mossy fiber synapses. By regulating information flow in the DG-CA3 circuit, preNMDARs may play a significant role in learning and memory.

Early studies using immunoperoxidase electron microscopy revealed NMDARs in presynaptic

compartments in multiple brain areas (for a review, see Corlew et al., 2008). Subsequent studies that used immunogold electron microscopy, a more precise localization method, identified NMDARs on the presynaptic membrane in a number of brain structures, including neocortex (Fujisawa & Aoki, 2003; Larsen et al., 2011), hippocampus (Berg, Larsson, Morland, & Gundersen, 2013; Jourdain et al., 2007; McGuinness et al., 2010), and amygdala (Pickel, Colago, Mania, Molosh, & Rainnie, 2006). In agreement with these studies, and using a previously validated antibody (Siegel et al., 1994), we identified prominent presynaptic labeling of the obligatory subunit GluN1 in mossy fiber boutons (Figure 1A-D). Moreover, we found that these receptors are close to the active zone and therefore well positioned to modulate neurotransmitter release.

Previous work in the cerebellum and neocortex suggested that somatodendritic potentials generated by NMDARs could signal to nerve terminals and lead to presynaptic Ca^{2+} elevations (Christie & Jahr, 2008, 2009). Thus, changes in neurotransmitter release resulting from NMDAR antagonism could be due to somatodendritic NMDARs but not necessarily preNMDARs residing on nerve terminals (Duguid, 2013). However, focal NMDAR antagonism far from the somatodendritic compartment and in transected axons still reduced short-term plasticity at mossy fiber synapses (Figure 3), making it extremely unlikely that somatodendritic NMDARs could explain our results. In further support of functional preNMDARs at mossy fibers, we found that 2PU of glutamate induced Ca^{2+} rise in control but not in GluN1-deficient boutons. Together, our findings strongly support the presence of functional preNMDARs facilitating neurotransmission at mf-CA3 synapses. Remarkably, the somatodendritic compartment of GCs can generate sub-threshold depolarizations at mossy fiber terminals (a.k.a. excitatory presynaptic potentials) (Alle & Geiger, 2006). By alleviating the magnesium blockade, these potentials could transiently boost the functional impact of mossy fiber preNMDARs.

While the presence of preNMDARs is downregulated during development both in neocortex (Corlew, Wang, Ghermazien, Erisir, & Philpot, 2007; Larsen et al., 2011) and hippocampus (Mameli, Carta, Partridge, & Valenzuela, 2005), we were able to detect functional preNMDARs in young adult rats (P17-P28) and mice (P30-P44), once mossy fiber connections are fully developed (Amaral & Dent, 1981). Functional preNMDARs have been identified in axonal growth cones of hippocampal and neocortical neurons, suggesting these receptors are important for regulating early synapse formation (Gill et al., 2015; Wang, Petralia, Wang, Wenthold, & Brenowitz, 2011). Because GCs undergo adult neurogenesis, and adult born GCs establish new connections in the mature brain, preNMDARs could also play an important role in immature mossy fiber synapses and functional integration of new born GCs into the mature hippocampus (Toni & Schinder, 2015). Moreover, experience can modulate the expression and composition of preNMDARs in neocortex (Larsen et al., 2014), a possibility not investigated in our study.

The glutamate that activates preNMDARs may originate from the presynaptic terminal, the postsynaptic cell, nearby synapses or neighboring glial cells. Our results indicate that activation of preNMDARs at mossy fiber synapses requires activity-dependent release of glutamate that likely arises from mossy fiber boutons, although other sources cannot be discarded, including astrocytes. At medial entorhinal inputs to GCs, preNMDARs appear to be localized away from the presynaptic release sites and facing astrocytes, consistent with preNMDAR activation by gliotransmitters (Jourdain et al., 2007; Savtchouk et al., 2019). In contrast, at mf-CA3 synapses we found that preNMDARs are adjacent to the release sites suggesting a direct control on glutamate release from mossy fiber boutons.

The precise mechanism by which preNMDARs facilitate neurotransmitter release is poorly understood but it may include Ca^{2+} influx through the receptor and depolarization of the presynaptic terminal with subsequent activation of voltage-gated calcium channels (Banerjee et

al., 2016; Corlew et al., 2008). In support of this mechanism is the high Ca^{2+} permeability of NMDARs (Paoletti et al., 2013; Rogers & Dani, 1995). Besides, presynaptic subthreshold depolarization and subsequent activation of presynaptic voltage-gated calcium channels is a common mechanism by which presynaptic ionotropic receptors facilitate neurotransmitter release (Engelman & MacDermott, 2004; Pinheiro & Mulle, 2008). PreNMDARs may also act in a metabotropic manner (Dore, Aow, & Malinow, 2016) and facilitate transmitter release in a Ca^{2+}-influx-independent manner (Abrahamsson et al., 2017). Our findings demonstrating that the open channel blocker MK-801 robustly reduced short-term plasticity at mossy fiber synapses support an ionotropic mechanism that involves calcium influx through preNMDARs. In line with previous studies that detected presynaptic Ca^{2+} rises following local activation of NMDARs (e.g. NMDA or glutamate uncaging) in visual cortex (Buchanan et al., 2012) and cerebellum (Rossi et al., 2012), we provide direct evidence that preNMDAR activation either by repetitive activation of mossy fibers or 2PU of glutamate increases presynaptic Ca^{2+} (Figures 5 and 6). Although the calcium targets remain unidentified, these may include proteins of the release machinery, calcium-dependent protein kinases and phosphatases, and calcium release from internal stores (Banerjee et al., 2016). In addition to facilitating evoked neurotransmitter release, preNMDARs can promote spontaneous neurotransmitter release as indicated by changes in miniature, action potential-independent activity (e.g. mEPSCs) (for recent reviews, see Banerjee et al., 2016; Kunz, Roberts, & Philpot, 2013; Wong et al., 2020). A potential role for preNMDARs in spontaneous, action potential-independent release at mossy fiber synapses cannot be discarded.

Our results show that activation of preNMDARs by physiologically relevant patterns of presynaptic activity enhanced mossy fiber transmission and DG-CA3 information transfer (Figure 4). Studies found NMDAR genetic deletion in GCs resulted in memory deficits (e.g. pattern separation) (McHugh et al., 2007). Although the mechanism is unclear, it could involve activity-dependent preNMDAR regulation of mossy fiber excitatory connections. We found that preNMDARs facilitate

neurotransmitter release in a target cell-specific manner. Like in neocortex (Larsen & Sjostrom, 2015), such specificity strongly suggests that preNMDARs have distinct roles in controlling information flow in cortical microcircuits. Thus, preNMDAR facilitation of mossy fiber synapses onto glutamatergic neurons but not GABAergic interneurons (Figure 8) may fine-tune the CA3 circuit by increasing the excitatory/inhibitory balance.

Given the multiple signaling cascades known to regulate NMDARs (Lau & Zukin, 2007; Sanz-Clemente, Nicoll, & Roche, 2013), preNMDARs at mossy fiber synapses may provide an important site of neuromodulatory control. PreNMDARs have been implicated in the induction of LTP and LTD at excitatory or inhibitory synapses in several brain areas (Banerjee et al., 2016; Wong et al., 2020). While most evidence, at least using robust induction protocols *in vitro,* indicates that long-term forms of presynaptic plasticity at mossy fiber synapses can occur in the absence of NMDAR activation (Castillo, 2012; Nicoll & Schmitz, 2005), our findings do not discard the possibility that preNMDARs could play a role *in vivo* during subtle presynaptic activities. As previously reported for corticostriatal LTP (Park et al., 2014), preNMDARs could regulate long-term synaptic plasticity by controlling BDNF release (Figure 7), which is consistent with BDNF-TrkB signaling being implicated in mf-CA3 LTP (Schildt, Endres, Lessmann, & Edelmann, 2013). In addition, BDNF could facilitate glutamate release by enhancing preNMDAR function (W. Chen et al., 2014; Madara & Levine, 2008). By potentiating mf-CA3 transmission, BDNF could also promote epileptic activity (McNamara & Scharfman, 2012). Lastly, dysregulation of NMDARs is commonly implicated in the pathophysiology of brain disorders such as schizophrenia, autism, and epilepsy (Lau & Zukin, 2007; Paoletti et al., 2013). PreNMDAR expression and function have been suggested to be altered in experimental models of disease, including neuropathic pain (Y. Chen, Chen, Chen, Zhang, & Pan, 2019; Zeng, Thomson, Aicher, & Terman, 2006), and epilepsy (Yang, Woodhall, & Jones, 2006). At present, however, *in vivo* evidence for the involvement of preNMDARs in brain function and disease is rather indirect (Bouvier et al., 2015; Wong et al.,

2020). The development of specific preNMDAR tools is required to determine the functional impact of these receptors *in vivo*.

Methods

Antibodies

A monoclonal antibody against GluN1 (clone 54.1 MAB363) was obtained from Millipore (Germany) and its specificity was characterized previously (Siegel et al., 1994). An affinity-purified polyclonal rabbit anti-GluA1-4 (pan-AMPA), corresponding to aa 724–781 of rat, was used and characterised previously (Nusser et al., 1998).

Immunohistochemistry for electron microscopy

Immunohistochemical reactions at the electron microscopic level were carried out using the post-embedding immunogold method as described earlier (Lujan, Nusser, Roberts, Shigemoto, & Somogyi, 1996). Briefly, animals (n = 3 rats were anesthetized by intraperitoneal injection of ketamine-xylazine 1:1 (0.1 mL/kg b.w.) and transcardially perfused with ice-cold fixative containing 4% paraformaldehyde, 0.1% glutaraldehyde and 15% saturated picric acid solution in 0.1 M phosphate buffer (PB) for 15 min. Vibratome sections 500 µm thick were placed into 1 M sucrose solution in 0.1 M PB for 2 h before they were slammed on a Leica EM CPC apparatus. Samples were dehydrated in methanol at -80°C and embedded by freeze-substitution (Leica EM AFS2) in Lowicryl HM 20 (Electron Microscopy Science, Hatfield, USA), followed by polimerization with UV light. Then, ultrathin 80-nm-thick sections from Lowicryl-embedded blocks of the hippocampus were picked up on coated nickel grids and incubated on drops of a blocking solution consisting of 2% human serum albumin in 0.05 M TBS and 0.03% Triton X-100. The grids were incubated with GluN1 or pan-AMPA antibodies (10 µg/mL in 0.05 M TBS and 0.03% Triton X-100 with 2% human serum albumin) at 28 °C overnight. The grids were incubated on drops of goat anti-rabbit IgG conjugated to 10 nm colloidal gold particles (Nanoprobes Inc.) in 2% human serum albumin and 0.5% polyethylene glycol in 0.05 M TBS and 0.03% Triton X-100. The grids were then washed in TBS and counterstained for electron microscopy with 1% aqueous uranyl acetate followed by Reynolds's lead citrate. Ultrastructural analyses were performed in a JEOL-1010 electron microscope.

468 **Hippocampal slice preparation**

469 Animal handling followed an approved protocol by the Albert Einstein College of Medicine
470 Institutional Animal Care and Use Committee in accordance with National Institute of Health
471 guidelines. Acute hippocampal slices (400 µm thick) were obtained from Sprague-Dawley rats
472 postnatal day 17 (P17) to P28 of either sex. The hippocampi were isolated and cut using a
473 VT1200s microslicer (Leica Microsystems Co.) in a solution containing (in mM): 215 sucrose, 2.5
474 KCl, 26 $NaHCO_3$, 1.6 NaH_2PO_4, 1 $CaCl_2$, 4 $MgCl_2$, 4 $MgSO_4$ and 20 glucose. Acute slices were
475 placed in a chamber containing a 1:1 mix of sucrose cutting solution and extracellular artificial
476 cerebrospinal fluid (ACSF) recording solution containing (in mM): 124 NaCl, 2.5 KCl, 26 $NaHCO_3$,
477 1 NaH_2PO_4, 2.5 $CaCl_2$, 1.3 $MgSO_4$ and 10 glucose incubated in a warm-water bath at 33-34˚C.
478 The chamber was brought to room temperature for at least 15 min post-sectioning and the 1:1
479 sucrose-ACSF solution was replaced by ACSF. All solutions were equilibrated with 95% O_2 and
480 5% CO_2 (pH 7.4). Slices were allowed to recover for at least 45 min in the ACSF solution before
481 recording.
482
483 **Electrophysiology**
484 Electrophysiology experiments were performed at 26.0 ± 0.1˚C in a submersion-type recording
485 chamber perfused at 2 ml/min with ACSF supplemented with the $GABA_A$ receptor antagonist
486 picrotoxin (100 µM) and the selective AMPA receptor (AMPAR) antagonist LY303070 at a low
487 concentration (0.5 µM) to minimize CA3-CA3 recurrent activity, or at a high concentration (15 µM)
488 to isolate KAR-EPSCs and KAR-EPSPs to assess monosynaptic mossy fiber transmission.
489 Whole-cell recordings were made from CA3 pyramidal cells voltage clamped at -70 mV using
490 patch-type pipette electrodes (3-4 mΩ) containing (in mM): 131 cesium gluconate, 8 NaCl, 1
491 $CaCl_2$, 10 EGTA, 10 glucose, 10 HEPES, and 2 MK-801 pH 7.25 (280-285 mOsm) unless
492 specified otherwise. KOH was used to adjust pH. Series resistance (8-15 MΩ) was monitored
493 throughout all experiments with a -5 mV, 80 ms voltage step, and cells that exhibited a series
494 resistance change (>20%) were excluded from analysis. A stimulating bipolar electrode (theta
495 glass, Warner Instruments) was filled with ACSF and placed in *stratum lucidum* to selectively
496 activate mossy fibers using a DS2A Isolated Voltage Stimulator (Digitimer Ltd.) with a 100 µs
497 pulse width duration. AMPAR-EPSCs were recorded for a baseline period of two minutes and
498 low-frequency facilitation (LFF) was induced by stepping the stimulation frequency from 0.1 to 1
499 Hz for two minutes. Facilitation was measured by taking a ratio of the mean EPSC during the
500 steady-state, LFF period of activity and the two minute baseline ($EPSC_{1Hz}/EPSC_{0.1Hz}$) before and
501 after bath-application of NMDAR antagonists.

To qualify for analysis, mossy fiber responses met three criteria: 1) The 20-80% rise time of the AMPAR-EPSC was less than 1 ms 2) LFF was greater than 150% 3) The AMPAR-EPSC displayed at least 70% sensitivity to the group 2/3 mGluR agonist, DCG-IV (1 μM). Isolated KAR-EPSCs were elicited by 2 pulses with a 5 ms inter-stimulus-interval for LFF experiments. Baseline measurements were acquired at least 10 min after "break-in" to achieve optimal intracellular blockade of postsynaptic NMDARs by MK-801 (2 mM) in the patch-pipette. To transect mossy fiber axons in acute slices, a 45˚ ophthalmic knife (Alcon Surgical) was used to make a diagonal cut across the hilus from the dorsal to ventral blades of the DG, and the subregion CA3b was targeted for patch-clamp recordings. For D-APV (2 mM) puff experiments, a puffer device (Toohey Company) was set to deliver 2-3 puffs of 100 ms duration at 3-4 psi during the two minutes of LFF activity. The puffer pipette was placed at least 300 μm away from the recording site and both the puff pipette and hippocampal slice were positioned to follow the direction of the laminar flow in the low profile, submersion-type chamber (RC-26GLP, Warner Instruments). Burst-induced facilitation was elicited by 5 pulses at 25 Hz with a 0.03 Hz inter-trial-interval for a baseline period of 10 min. Facilitation was measured by taking a ratio of the mean KAR-EPSC peak of the 5^{th} pulse to the 1^{st} pulse (P_5/P_1) before and after bath-application of MK-801 (50 μM). To study KAR induced action potentials, CA3 pyramidal cells were patch-clamped with internal solution containing in (mM): 112 potassium gluconate, 17 KCl, 0.04 $CaCl_2$, 0.1 EGTA, 10 HEPES, 10 NaCl, 2 MgATP, 0.2 Na_3GTP and 2 MK-801, pH 7.2 (280-285 mOsm). Current-clamped CA3 cells were held at -70 mV during burst stimulation of mossy fibers (5 pulses at 25 Hz) to monitor action potentials. Spike-transfer was measured by mean spikes/burst quantified for a 10 min period before and after bath application of MK-801 (50 μM). Robust sensitivity to the AMPAR/KAR selective antagonist NBQX (10 μM) confirmed KAR-EPSC responses. Both hilar mossy cells and CA3 interneurons were visually patched-loaded with Alexa 594 (35 μM) and morphological identity was confirmed by two-photon imaging at the end of experiments. Hilar mossy cells were voltage clamped at -70 mV and a bipolar electrode was placed in the DG to activate mossy fibers. The data analysis and inclusion criteria used for mossy fiber experiments was also implemented for hilar mossy cell recordings. CA3 interneurons were voltage clamped at -70 mV and burst-stimulated, facilitation was assessed as previously mentioned. Both facilitating and depressing mossy fiber responses were included for analysis given the diversity of mossy fiber-CA3 interneuron transmission (Toth et al., 2000). Whole-cell voltage and current clamp recordings were performed with an Axon MultiClamp 700B amplifier (Molecular Devices). Signals were

filtered at 2 kHz and digitized at 5 kHz. Stimulation and acquisition were controlled with custom software (Igor Pro 6).

Transgenic animals

Grn1-floxed littermate mice of either sex (P16-20) were injected with 1 µl of AAV5-CamKII-eGFP, AAV5-CamKII-CreGFP, AAV5-CamKII-mcherry, or AAV5-CamKII-mcherry-Cre viruses at a rate of 0.12 µl/min at coordinates (±1.9 mm A/P, ±1.1 mm M/L, ±2.4 mm D/V) targeting the DG using a stereotaxic apparatus (Kopf Instruments). Two weeks post-surgery mice were sacrificed for electrophysiology or calcium imaging experiments. Mice were perfused with 20 ml of cold NMDG solution containing in (mM): 93 NMDG, 2.5 KCl, 1.25 NaH_2PO_4, 30 $NaHCO_3$, 20 HEPES, 25 glucose, 5 sodium ascorbate, 2 Thiourea, 3 sodium pyruvate, 10 $MgCl_2$, 0.5 $CaCl_2$, brought to pH 7.35 with HCl. The hippocampi were isolated and cut using a VT1200s microslicer in cold NMDG solution. Acute mouse slices were placed in a chamber containing ACSF solution that was incubated in a warm water bath 33-34 ˚C. All solutions were equilibrated with 95% O_2 and 5% CO_2 (pH 7.4). Post-sectioning, slices were allowed to recover at room temperature for at least 45 min prior to experiments. For NMDAR/AMPAR ratios, GCs were patch-clamped with the cesium internal solution previously mentioned containing either Alexa 594 (35 µM) for GFP+ cells (laser tuned to 830 nm/910 nm, respectively) or Alexa 488 (35 µM) for mCherry+ cells (laser tuned to 910 nm/780 nm, respectively). AMPAR-EPSCs were recorded at -65 mV in the presence of picrotoxin (100 µM) by placing a bipolar electrode near the medial perforant path and delivering a 100 µs pulse width duration using an Isoflex stimulating unit. AMPAR-EPSCs were acquired for at least 5 min followed by bath-application of NBQX (10 µM) to isolate NMDAR-EPSCs. GCs were brought to +40 mV to alleviate magnesium block and record optimal NMDAR-EPSCs. NMDAR/AMPAR ratios were measured by taking the mean NMDAR-EPSC/AMPAR-EPSC for a 5 min period of each component. Only acute mouse slices with optimal GFP and mCherry reporter fluorescence (i.e. robust expression) were used for electrophysiology and calcium imaging experiments. *Grin1*-floxed animals (The Jackson Laboratory) were kindly provided by Dr. Michael Higley (Yale University).

Optogenetics

Grin1 floxed and control mice of either sexes (P17-20) were injected with a 1:2 mix of AAV5-CamKII-CreGFP/AAV-DJ-FLEX-ChiEF-tdTomato viruses targeting the DG. At least four weeks post-surgery acute hippocampal slices were prepared as previously described and slices showing optimal GFP and tdTomato expression were used for electrophysiology experiments. Mossy fiber

optical burst-stimulation was elicited by using a Coherent 473 nm laser (4-8 mW) delivering 5 pulses at 25 Hz with a 1-2 ms pulse width duration. Facilitation was measured by taking a ratio of the mean AMPAR-EPSC peak of the 5th pulse to the 1st pulse (P_5/P_1) in control and *Grin1*-cKO animals.

Two-photon calcium imaging and MNI-glutamate uncaging

mCherry+ GCs were patch-loaded with an internal solution containing in (mM): 130 $KMeSO_4$, HEPES, $MgCl_2$, Na_2ATP, NaGTP, phosphocreatine, .035 Alexa 594, and .2 Fluo-5F. GCs near the hilar border were avoided and GCs that exhibited adult-born GCs properties were excluded from analysis. The cells were kept in voltage clamp configuration at -50 mV for at least 1 hr to allow the diffusion of dyes to mossy fiber boutons in ACSF solution containing in (mM): 124 NaCl, 2.5 KCl, 26 $NaHCO_3$, 1 NaH_2PO_4, 4 $CaCl_2$, 0 $MgSO_4$, 10 glucose, 0.01 NBQX, 0.1 picrotoxin, and 0.01 D-serine. Using an Ultima 2P microscope (Bruker Corp) with and Insight Deep See laser (Spectra Physics) tuned to 830 nm the "red" PMT was turned on and with minimal pockel power the red signal was used to identify the mossy fiber axon. With 512 x 512 pixel resolution mossy fiber axons were followed for at least 200 µm until bouton structures were morphologically identified and measured at least 3 µm in diameter. GCs were switched to current clamp mode held at -70 mV and 1 ms current injections were used to elicit a burst of 5 action potentials at 25 Hz. Using line scan analysis software (PrairieView 5.4, Bruker Corp.) a line was drawn across the diameter of the bouton at a magnification of at least 16X. The “green” PMT channel was turned on and 1,000 lines were acquired in a 2 sec time period. Action potential induction was delayed for 400 ms to collect a baseline fluorescence time period. Calcium transients (CaTs) were acquired with a 1 min inter-trial-interval and analyzed using the ΔG/R calculation. CaTs from control animals were compared to *Grin1*-cKO by taking the mean peak ΔG/R value for a 30 ms period of the 5th action potential.

For uncaging experiments GCs that were mCherry+ were patch-loaded using the internal solution previously described in the presence of a 12 ml ACSF solution containing in (mM): 124 NaCl, 2.5 KCl, 26 $NaHCO_3$, 1 NaH_2PO_4, 4 $CaCl_2$, 0 $MgSO_4$, 10 glucose, 2.5 MNI-glutamate, 0.01 NBQX, 0.1 picrotoxin, and 0.01 D-serine that was recirculated in a submersion type chamber. A MaiTai HP laser (Spectra Physics) was tuned to 720 nm to optimally uncage glutamate and elicit CaTs in GC spines. Following successful CaTs in GC spines, mossy fiber boutons were identified and to mimic bursting activity, 5 uncaging pulses (1 ms duration) were delivered at 25 Hz. The

602 acquired CaTs in spines and boutons were analyzed using the ΔG/R calculation in control and
603 *Grin1*-cKO animals.
604
605 **Two-photon BDNF-phluorin imaging**
606 *Grin1* floxed and control mice of both sexes (P16-20) were injected with a 1:2 mix of AAV5-
607 CamKII-mCherryCre/AAV-DJ-DIO-BDNF-phluorin viruses targeting the DG. At least four weeks
608 post-surgery acute hippocampal slices were prepared as previously described and slices showing
609 optimal GFP and mCherry expression were taken for imaging sessions. Briefly, a stimulating
610 monopolar micropipette electrode was placed in the *stratum lucidum* at least 250 μm away from
611 the imaging site. The Insight Deep See laser (Spectra Physics) was tuned to 880 nm and the
612 imaging site was selected by the appearance of fibers and bouton structures in the *stratum*
613 *lucidum*. Using 512 X 512 pixel resolution identified boutons measuring at least 3 μm in diameter
614 were selected as a region of interest (ROI) magnified to 4-6X and a baseline acquisition of 100
615 consecutive images at 1 Hz using T-series software (PrairieView 5.4, Bruker Corp.) was acquired
616 (Park et al., 2014). Following the baseline acquisition a burst-stimulation consisting of 125 pulses
617 at 25 Hz was delivered 2x, triggering an acquisition of 200 consecutive images at 1 Hz. The
618 fluorescence intensity of the bouton ROI was measured using ImageJ software to calculate ΔF/F
619 of the BDNF-pHluorin signal. To verify reactivity of the ROI an isosmotic solution of NH_4Cl (50
620 mM) was added at the end of the imaging session as previously reported (Park et al., 2014).
621
622 **Viruses**
623 AAV5-CamKII-eGFP and AAV5-CamKII-CreGFP viruses were acquired from UPenn Vector Core.
624 AAV5-CamKII-mcherry and AAV5-CamKII-mcherry-Cre were obtained from UNC Chapel Hill
625 Vector Core. The AAV-DJ-FLEX-ChiEF-tdTomato and AAV-DJ-DIO-BDNF-phluorin viruses were
626 custom ordered and obtained from UNC Chapel Hill Vector Core. The DNA of the ChiEF virus
627 was a generous gift from Dr. Pascal Kaeser (Harvard University), and the DNA of the BDNF-
628 pHluorin was kindly provided by Dr. Hyungju Park (Korea Brain Research Institute).
629
630 **Chemicals & Drugs**
631 Picrotoxin and all chemicals used to prepare cutting, recording, and internal solutions were
632 acquired from Sigma-Aldrich. All NMDAR antagonists (D-APV, MK-801, R-CPP), NMDAR agonist
633 (D-serine), and the group 2/3 mGluR agonist (DCG-IV) were purchased from Tocris. D-APV was
634 also acquired from the NIMH Chemical Synthesis Drug Program. NBQX was purchased from
635 Cayman Chemical Company. The noncompetitive AMPAR selective antagonist LY303070 was

custom ordered from ABX Chemical Company. Alexa 594 morphological dye and the calcium indicator Fluo-5F were purchased from Thermo Scientific. For uncaging experiments MNI-glutamate was ordered from Tocris.

Statistical analysis and Data Acquisition

All data points from experiments were tested for normality using a Shapiro-Wilk test where the p value was set to < 5% for a normal distribution. Experiments with a normal distribution and an N > to 7 cells were tested for statistical significance with a paired Student *t*-test with p value set to < 5%. Experiments with N < 7 cells or skewed distributions were tested for statistical significance using a paired Wilcoxon signed rank sum test with p value set to < 5%. For experiments comparing control and *Grin1*-cKO animals statistical significance was determined using Unpaired *t*-test and Mann-Whitney test with p values set to < 5% for normal distributions or rejected normality, respectively. All statistical tests were calculated using Origin Pro 9 (Origin Lab). Experimenters were blind to the identity of the virus injected in transgenic *Grin1* floxed mice during the acquisition of data in CA3 electrophysiology and two-photon imaging. However, data analysis could not be performed blind in those experiments in which NMDAR/AMPAR ratios in GCs were examined in order to assess the efficiency of the cKO.

Acknowledgements: We thank current and former lab members for invaluable discussions, in particular Hannah Monday, Chiayu Chiu, Coralie Berthoux and Kaoutsar Nasrallah for critical evaluation of the manuscript. We also thank Dr. Hyungju Park for his generous gift of the BDNF-pHluorin DNA construct, Dr. Michael Higley for sharing *Grin1* floxed mice, and Dr. Pascal Kaeser for his generous gift of the Cre-dependent ChIEF DNA construct. This work supported by the NIH (F31-MH109267 to PJL; R01-DA17392, R01 MH116673, R01MH125772, R01 MH081935, and to P.E.C.) and by the Spanish Ministerio de Economia y Competitividad (RTI2018-095812-B-I00) and Junta de Comunidades de Castillo-La Mancha (SBPLY/17/180501/000229) to RL.

The authors declare no competing financial interests.

Author Contributions: PJL and PEC designed the experiments. PJL performed experiments and analyzed data. HBK performed preliminary experiments and made observations that triggered this study. RL performed EM experiments and analyzed the data. PJL and PEC wrote the first manuscript which was edited by all authors.

677 **REFERENCES**
678
679 Abbott, L. F., & Regehr, W. G. (2004). Synaptic computation. *Nature, 431*(7010), 796-803.
680 doi:10.1038/nature03010
681 Abrahamsson, T., Chou, C. Y. C., Li, S. Y., Mancino, A., Costa, R. P., Brock, J. A., . . . Sjostrom,
682 P. J. (2017). Differential Regulation of Evoked and Spontaneous Release by Presynaptic
683 NMDA Receptors. *Neuron, 96*(4), 839-855 e835. doi:10.1016/j.neuron.2017.09.030
684 Alle, H., & Geiger, J. R. (2006). Combined analog and action potential coding in hippocampal
685 mossy fibers. *Science, 311*(5765), 1290-1293. doi:10.1126/science.1119055
686 Amaral, D. G., & Dent, J. A. (1981). Development of the mossy fibers of the dentate gyrus: I. A
687 light and electron microscopic study of the mossy fibers and their expansions. *J Comp*
688 *Neurol, 195*(1), 51-86. doi:10.1002/cne.901950106
689 Amaral, D. G., Scharfman, H. E., & Lavenex, P. (2007). The dentate gyrus: fundamental
690 neuroanatomical organization (dentate gyrus for dummies). *Prog Brain Res, 163*, 3-22.
691 doi:S0079-6123(07)63001-5 [pii] 10.1016/S0079-6123(07)63001-5
692 Banerjee, A., Larsen, R. S., Philpot, B. D., & Paulsen, O. (2016). Roles of Presynaptic NMDA
693 Receptors in Neurotransmission and Plasticity. *Trends Neurosci, 39*(1), 26-39.
694 doi:10.1016/j.tins.2015.11.001
695 Berg, L. K., Larsson, M., Morland, C., & Gundersen, V. (2013). Pre- and postsynaptic localization
696 of NMDA receptor subunits at hippocampal mossy fibre synapses. *Neuroscience, 230*,
697 139-150. doi:10.1016/j.neuroscience.2012.10.061
698 Berretta, N., & Jones, R. S. (1996). Tonic facilitation of glutamate release by presynaptic N-methyl-
699 D-aspartate autoreceptors in the entorhinal cortex. *Neuroscience, 75*(2), 339-344.
700 doi:10.1016/0306-4522(96)00301-6
701 Bischofberger, J., Engel, D., Frotscher, M., & Jonas, P. (2006). Timing and efficacy of transmitter
702 release at mossy fiber synapses in the hippocampal network. *Pflugers Arch, 453*(3), 361-
703 372. doi:10.1007/s00424-006-0093-2
704 Bouvier, G., Bidoret, C., Casado, M., & Paoletti, P. (2015). Presynaptic NMDA receptors: Roles
705 and rules. *Neuroscience, 311*, 322-340. doi:10.1016/j.neuroscience.2015.10.033
706 Bouvier, G., Higgins, D., Spolidoro, M., Carrel, D., Mathieu, B., Lena, C., . . . Casado, M. (2016).
707 Burst-Dependent Bidirectional Plasticity in the Cerebellum Is Driven by Presynaptic NMDA
708 Receptors. *Cell Rep, 15*(1), 104-116. doi:10.1016/j.celrep.2016.03.004
709 Bouvier, G., Larsen, R. S., Rodriguez-Moreno, A., Paulsen, O., & Sjostrom, P. J. (2018). Towards
710 resolving the presynaptic NMDA receptor debate. *Curr Opin Neurobiol, 51*, 1-7.
711 doi:10.1016/j.conb.2017.12.020
712 Buchanan, K. A., Blackman, A. V., Moreau, A. W., Elgar, D., Costa, R. P., Lalanne, T., . . . Sjostrom,
713 P. J. (2012). Target-specific expression of presynaptic NMDA receptors in neocortical
714 microcircuits. *Neuron, 75*(3), 451-466. doi:10.1016/j.neuron.2012.06.017
715 Burke, K. J., Jr., & Bender, K. J. (2019). Modulation of Ion Channels in the Axon: Mechanisms
716 and Function. *Front Cell Neurosci, 13*, 221. doi:10.3389/fncel.2019.00221
717 Carter, B. C., & Jahr, C. E. (2016). Postsynaptic, not presynaptic NMDA receptors are required
718 for spike-timing-dependent LTD induction. *Nat Neurosci, 19*(9), 1218-1224.
719 doi:10.1038/nn.4343
720 Castillo, P. E. (2012). Presynaptic LTP and LTD of excitatory and inhibitory synapses. *Cold Spring*
721 *Harb Perspect Biol, 4*(2). doi:10.1101/cshperspect.a005728
722 Castillo, P. E., Malenka, R. C., & Nicoll, R. A. (1997). Kainate receptors mediate a slow
723 postsynaptic current in hippocampal CA3 neurons. *Nature, 388*(6638), 182-186.
724 doi:10.1038/40645
725 Chamberland, S., Timofeeva, Y., Evstratova, A., Volynski, K., & Toth, K. (2018). Action potential
726 counting at giant mossy fiber terminals gates information transfer in the hippocampus.
727 *Proc Natl Acad Sci U S A, 115*(28), 7434-7439. doi:10.1073/pnas.1720659115

728 Chen, W., Walwyn, W., Ennes, H. S., Kim, H., McRoberts, J. A., & Marvizon, J. C. (2014). BDNF
729 released during neuropathic pain potentiates NMDA receptors in primary afferent
730 terminals. *Eur J Neurosci, 39*(9), 1439-1454. doi:10.1111/ejn.12516
731 Chen, Y., Chen, S. R., Chen, H., Zhang, J., & Pan, H. L. (2019). Increased alpha2delta-1-NMDA
732 receptor coupling potentiates glutamatergic input to spinal dorsal horn neurons in
733 chemotherapy-induced neuropathic pain. *J Neurochem, 148*(2), 252-274.
734 doi:10.1111/jnc.14627
735 Christie, J. M., & Jahr, C. E. (2008). Dendritic NMDA receptors activate axonal calcium channels.
736 *Neuron, 60*(2), 298-307. doi:10.1016/j.neuron.2008.08.028
737 Christie, J. M., & Jahr, C. E. (2009). Selective expression of ligand-gated ion channels in L5
738 pyramidal cell axons. *J Neurosci, 29*(37), 11441-11450. doi:10.1523/JNEUROSCI.2387-
739 09.2009
740 Conner, J. M., Lauterborn, J. C., Yan, Q., Gall, C. M., & Varon, S. (1997). Distribution of brain-
741 derived neurotrophic factor (BDNF) protein and mRNA in the normal adult rat CNS:
742 evidence for anterograde axonal transport. *J Neurosci, 17*(7), 2295-2313.
743 Corlew, R., Brasier, D. J., Feldman, D. E., & Philpot, B. D. (2008). Presynaptic NMDA receptors:
744 newly appreciated roles in cortical synaptic function and plasticity. *Neuroscientist, 14*(6),
745 609-625. doi:10.1177/1073858408322675
746 Corlew, R., Wang, Y., Ghermazien, H., Erisir, A., & Philpot, B. D. (2007). Developmental switch in
747 the contribution of presynaptic and postsynaptic NMDA receptors to long-term depression.
748 *J Neurosci, 27*(37), 9835-9845. doi:10.1523/JNEUROSCI.5494-06.2007
749 Cull-Candy, S., Brickley, S., & Farrant, M. (2001). NMDA receptor subunits: diversity, development
750 and disease. *Curr Opin Neurobiol, 11*(3), 327-335.
751 Diamantaki, M., Frey, M., Berens, P., Preston-Ferrer, P., & Burgalossi, A. (2016). Sparse activity
752 of identified dentate granule cells during spatial exploration. *Elife, 5*.
753 doi:10.7554/eLife.20252
754 Dore, K., Aow, J., & Malinow, R. (2016). The Emergence of NMDA Receptor Metabotropic
755 Function: Insights from Imaging. *Front Synaptic Neurosci, 8*, 20.
756 doi:10.3389/fnsyn.2016.00020
757 Duguid, I. C. (2013). Presynaptic NMDA receptors: are they dendritic receptors in disguise? *Brain*
758 *Res Bull, 93*, 4-9. doi:10.1016/j.brainresbull.2012.12.004
759 Duguid, I. C., & Smart, T. G. (2009). Presynaptic NMDA Receptors. In A. M. Van Dongen (Ed.),
760 *Biology of the NMDA Receptor*. Boca Raton (FL).
761 Engelman, H. S., & MacDermott, A. B. (2004). Presynaptic ionotropic receptors and control of
762 transmitter release. *Nat Rev Neurosci, 5*(2), 135-145. doi:10.1038/nrn1297
763 Evstratova, A., & Toth, K. (2014). Information processing and synaptic plasticity at hippocampal
764 mossy fiber terminals. *Front Cell Neurosci, 8*, 28. doi:10.3389/fncel.2014.00028
765 Fujisawa, S., & Aoki, C. (2003). In vivo blockade of N-methyl-D-aspartate receptors induces rapid
766 trafficking of NR2B subunits away from synapses and out of spines and terminals in adult
767 cortex. *Neuroscience, 121*(1), 51-63. doi:10.1016/s0306-4522(03)00341-5
768 Gill, I., Droubi, S., Giovedi, S., Fedder, K. N., Bury, L. A., Bosco, F., . . . Sabo, S. L. (2015).
769 Presynaptic NMDA receptors - dynamics and distribution in developing axons in vitro and
770 in vivo. *J Cell Sci, 128*(4), 768-780. doi:10.1242/jcs.162362
771 GoodSmith, D., Chen, X., Wang, C., Kim, S. H., Song, H., Burgalossi, A., . . . Knierim, J. J. (2017).
772 Spatial Representations of Granule Cells and Mossy Cells of the Dentate Gyrus. *Neuron,*
773 *93*(3), 677-690 e675. doi:10.1016/j.neuron.2016.12.026
774 Hagena, H., & Manahan-Vaughan, D. (2010). Frequency facilitation at mossy fiber-CA3 synapses
775 of freely behaving rats contributes to the induction of persistent LTD via an adenosine-A1
776 receptor-regulated mechanism. *Cereb Cortex, 20*(5), 1121-1130.
777 doi:10.1093/cercor/bhp184
778 Henze, D. A., Urban, N. N., & Barrionuevo, G. (2000). The multifarious hippocampal mossy fiber

779 pathway: a review. *Neuroscience, 98*(3), 407-427.
780 Henze, D. A., Wittner, L., & Buzsaki, G. (2002). Single granule cells reliably discharge targets in
781 the hippocampal CA3 network in vivo. *Nat Neurosci, 5*(8), 790-795. doi:10.1038/nn887
782 Jackman, S. L., & Regehr, W. G. (2017). The Mechanisms and Functions of Synaptic Facilitation.
783 *Neuron, 94*(3), 447-464. doi:10.1016/j.neuron.2017.02.047
784 Jourdain, P., Bergersen, L. H., Bhaukaurally, K., Bezzi, P., Santello, M., Domercq, M., . . . Volterra,
785 A. (2007). Glutamate exocytosis from astrocytes controls synaptic strength. *Nat Neurosci,*
786 *10*(3), 331-339. doi:10.1038/nn1849
787 Kamiya, H., Shinozaki, H., & Yamamoto, C. (1996). Activation of metabotropic glutamate receptor
788 type 2/3 suppresses transmission at rat hippocampal mossy fibre synapses. *J Physiol,*
789 *493 (Pt 2)*, 447-455. doi:10.1113/jphysiol.1996.sp021395
790 Klug, A., Borst, J. G., Carlson, B. A., Kopp-Scheinpflug, C., Klyachko, V. A., & Xu-Friedman, M.
791 A. (2012). How do short-term changes at synapses fine-tune information processing? *J*
792 *Neurosci, 32*(41), 14058-14063. doi:10.1523/JNEUROSCI.3348-12.2012
793 Kunz, P. A., Roberts, A. C., & Philpot, B. D. (2013). Presynaptic NMDA receptor mechanisms for
794 enhancing spontaneous neurotransmitter release. *J Neurosci, 33*(18), 7762-7769.
795 doi:10.1523/JNEUROSCI.2482-12.2013
796 Kwon, H. B., & Castillo, P. E. (2008). Role of glutamate autoreceptors at hippocampal mossy fiber
797 synapses. *Neuron, 60*(6), 1082-1094. doi:10.1016/j.neuron.2008.10.045
798 Larsen, R. S., Corlew, R. J., Henson, M. A., Roberts, A. C., Mishina, M., Watanabe, M., . . . Philpot,
799 B. D. (2011). NR3A-containing NMDARs promote neurotransmitter release and spike
800 timing-dependent plasticity. *Nat Neurosci, 14*(3), 338-344. doi:10.1038/nn.2750
801 Larsen, R. S., & Sjostrom, P. J. (2015). Synapse-type-specific plasticity in local circuits. *Curr Opin*
802 *Neurobiol, 35*, 127-135. doi:10.1016/j.conb.2015.08.001
803 Larsen, R. S., Smith, I. T., Miriyala, J., Han, J. E., Corlew, R. J., Smith, S. L., & Philpot, B. D.
804 (2014). Synapse-specific control of experience-dependent plasticity by presynaptic NMDA
805 receptors. *Neuron, 83*(4), 879-893. doi:10.1016/j.neuron.2014.07.039
806 Lau, C. G., & Zukin, R. S. (2007). NMDA receptor trafficking in synaptic plasticity and
807 neuropsychiatric disorders. *Nat Rev Neurosci, 8*(6), 413-426. doi:10.1038/nrn2153
808 Lawrence, J. J., & McBain, C. J. (2003). Interneuron diversity series: containing the detonation--
809 feedforward inhibition in the CA3 hippocampus. *Trends Neurosci, 26*(11), 631-640.
810 doi:10.1016/j.tins.2003.09.007
811 Lujan, R., Nusser, Z., Roberts, J. D., Shigemoto, R., & Somogyi, P. (1996). Perisynaptic location
812 of metabotropic glutamate receptors mGluR1 and mGluR5 on dendrites and dendritic
813 spines in the rat hippocampus. *Eur J Neurosci, 8*(7), 1488-1500.
814 Lysetskiy, M., Foldy, C., & Soltesz, I. (2005). Long- and short-term plasticity at mossy fiber
815 synapses on mossy cells in the rat dentate gyrus. *Hippocampus, 15*(6), 691-696.
816 doi:10.1002/hipo.20096
817 Madara, J. C., & Levine, E. S. (2008). Presynaptic and postsynaptic NMDA receptors mediate
818 distinct effects of brain-derived neurotrophic factor on synaptic transmission. *J*
819 *Neurophysiol, 100*(6), 3175-3184. doi:10.1152/jn.90880.2008
820 Mameli, M., Carta, M., Partridge, L. D., & Valenzuela, C. F. (2005). Neurosteroid-induced plasticity
821 of immature synapses via retrograde modulation of presynaptic NMDA receptors. *J*
822 *Neurosci, 25*(9), 2285-2294. doi:10.1523/JNEUROSCI.3877-04.2005
823 Martin, D., Bustos, G. A., Bowe, M. A., Bray, S. D., & Nadler, J. V. (1991). Autoreceptor regulation
824 of glutamate and aspartate release from slices of the hippocampal CA1 area. *J*
825 *Neurochem, 56*(5), 1647-1655. doi:10.1111/j.1471-4159.1991.tb02063.x
826 McGuinness, L., Taylor, C., Taylor, R. D., Yau, C., Langenhan, T., Hart, M. L., . . . Emptage, N. J.
827 (2010). Presynaptic NMDARs in the hippocampus facilitate transmitter release at theta
828 frequency. *Neuron, 68*(6), 1109-1127. doi:10.1016/j.neuron.2010.11.023
829 McHugh, T. J., Jones, M. W., Quinn, J. J., Balthasar, N., Coppari, R., Elmquist, J. K., . . .

Tonegawa, S. (2007). Dentate gyrus NMDA receptors mediate rapid pattern separation in the hippocampal network. *Science, 317*(5834), 94-99. doi:10.1126/science.1140263

McNamara, J. O., & Scharfman, H. E. (2012). Temporal Lobe Epilepsy and the BDNF Receptor, TrkB. In th, J. L. Noebels, M. Avoli, M. A. Rogawski, R. W. Olsen, & A. V. Delgado-Escueta (Eds.), *Jasper's Basic Mechanisms of the Epilepsies*. Bethesda (MD).

Miller, R. J. (1998). Presynaptic receptors. *Annu Rev Pharmacol Toxicol, 38*, 201-227. doi:10.1146/annurev.pharmtox.38.1.201

Nicoll, R. A., & Schmitz, D. (2005). Synaptic plasticity at hippocampal mossy fibre synapses. *Nat Rev Neurosci, 6*(11), 863-876. doi:10.1038/nrn1786

Nusser, Z., Lujan, R., Laube, G., Roberts, J. D., Molnar, E., & Somogyi, P. (1998). Cell type and pathway dependence of synaptic AMPA receptor number and variability in the hippocampus. *Neuron, 21*(3), 545-559.

Paoletti, P., Bellone, C., & Zhou, Q. (2013). NMDA receptor subunit diversity: impact on receptor properties, synaptic plasticity and disease. *Nat Rev Neurosci, 14*(6), 383-400. doi:10.1038/nrn3504

Park, H., Popescu, A., & Poo, M. M. (2014). Essential role of presynaptic NMDA receptors in activity-dependent BDNF secretion and corticostriatal LTP. *Neuron, 84*(5), 1009-1022. doi:10.1016/j.neuron.2014.10.045

Pernia-Andrade, A. J., & Jonas, P. (2014). Theta-gamma-modulated synaptic currents in hippocampal granule cells in vivo define a mechanism for network oscillations. *Neuron, 81*(1), 140-152. doi:10.1016/j.neuron.2013.09.046

Petralia, R. S., Yokotani, N., & Wenthold, R. J. (1994). Light and electron microscope distribution of the NMDA receptor subunit NMDAR1 in the rat nervous system using a selective anti-peptide antibody. *J Neurosci, 14*(2), 667-696.

Pickel, V. M., Colago, E. E., Mania, I., Molosh, A. I., & Rainnie, D. G. (2006). Dopamine D1 receptors co-distribute with N-methyl-D-aspartic acid type-1 subunits and modulate synaptically-evoked N-methyl-D-aspartic acid currents in rat basolateral amygdala. *Neuroscience, 142*(3), 671-690. doi:10.1016/j.neuroscience.2006.06.059

Pinheiro, P. S., & Mulle, C. (2008). Presynaptic glutamate receptors: physiological functions and mechanisms of action. *Nat Rev Neurosci, 9*(6), 423-436. doi:10.1038/nrn2379

Rebola, N., Carta, M., & Mulle, C. (2017). Operation and plasticity of hippocampal CA3 circuits: implications for memory encoding. *Nat Rev Neurosci, 18*(4), 208-220. doi:10.1038/nrn.2017.10

Rogers, M., & Dani, J. A. (1995). Comparison of quantitative calcium flux through NMDA, ATP, and ACh receptor channels. *Biophys J, 68*(2), 501-506. doi:10.1016/S0006-3495(95)80211-0

Rossi, B., Ogden, D., Llano, I., Tan, Y. P., Marty, A., & Collin, T. (2012). Current and calcium responses to local activation of axonal NMDA receptors in developing cerebellar molecular layer interneurons. *PLoS One, 7*(6), e39983. doi:10.1371/journal.pone.0039983

Salin, P. A., Scanziani, M., Malenka, R. C., & Nicoll, R. A. (1996). Distinct short-term plasticity at two excitatory synapses in the hippocampus. *Proc Natl Acad Sci U S A, 93*(23), 13304-13309.

Sanz-Clemente, A., Nicoll, R. A., & Roche, K. W. (2013). Diversity in NMDA receptor composition: many regulators, many consequences. *Neuroscientist, 19*(1), 62-75. doi:10.1177/1073858411435129

Savtchouk, I., Di Castro, M. A., Ali, R., Stubbe, H., Lujan, R., & Volterra, A. (2019). Circuit-specific control of the medial entorhinal inputs to the dentate gyrus by atypical presynaptic NMDARs activated by astrocytes. *Proc Natl Acad Sci U S A, 116*(27), 13602-13610. doi:10.1073/pnas.1816013116

Schicker, K. W., Dorostkar, M. M., & Boehm, S. (2008). Modulation of transmitter release via presynaptic ligand-gated ion channels. *Curr Mol Pharmacol, 1*(2), 106-129.

doi:10.2174/1874467210801020106

Schildt, S., Endres, T., Lessmann, V., & Edelmann, E. (2013). Acute and chronic interference with BDNF/TrkB-signaling impair LTP selectively at mossy fiber synapses in the CA3 region of mouse hippocampus. *Neuropharmacology, 71*, 247-254. doi:10.1016/j.neuropharm.2013.03.041

Senzai, Y., & Buzsaki, G. (2017). Physiological Properties and Behavioral Correlates of Hippocampal Granule Cells and Mossy Cells. *Neuron, 93*(3), 691-704 e695. doi:10.1016/j.neuron.2016.12.011

Siegel, S. J., Brose, N., Janssen, W. G., Gasic, G. P., Jahn, R., Heinemann, S. F., & Morrison, J. H. (1994). Regional, cellular, and ultrastructural distribution of N-methyl-D-aspartate receptor subunit 1 in monkey hippocampus. *Proc Natl Acad Sci U S A, 91*(2), 564-568.

Takumi, Y., Ramirez-Leon, V., Laake, P., Rinvik, E., & Ottersen, O. P. (1999). Different modes of expression of AMPA and NMDA receptors in hippocampal synapses. *Nat Neurosci, 2*(7), 618-624. doi:10.1038/10172

Toni, N., & Schinder, A. F. (2015). Maturation and Functional Integration of New Granule Cells into the Adult Hippocampus. *Cold Spring Harb Perspect Biol, 8*(1), a018903. doi:10.1101/cshperspect.a018903

Toth, K., Suares, G., Lawrence, J. J., Philips-Tansey, E., & McBain, C. J. (2000). Differential mechanisms of transmission at three types of mossy fiber synapse. *J Neurosci, 20*(22), 8279-8289.

Traynelis, S. F., Wollmuth, L. P., McBain, C. J., Menniti, F. S., Vance, K. M., Ogden, K. K., . . . Dingledine, R. (2010). Glutamate receptor ion channels: structure, regulation, and function. *Pharmacol Rev, 62*(3), 405-496. doi:10.1124/pr.109.002451

Vandael, D., Borges-Merjane, C., Zhang, X., & Jonas, P. (2020). Short-Term Plasticity at Hippocampal Mossy Fiber Synapses Is Induced by Natural Activity Patterns and Associated with Vesicle Pool Engram Formation. *Neuron, 107*(3), 509-521 e507. doi:10.1016/j.neuron.2020.05.013

Vyleta, N. P., Borges-Merjane, C., & Jonas, P. (2016). Plasticity-dependent, full detonation at hippocampal mossy fiber-CA3 pyramidal neuron synapses. *Elife, 5*. doi:10.7554/eLife.17977

Wang, P. Y., Petralia, R. S., Wang, Y. X., Wenthold, R. J., & Brenowitz, S. D. (2011). Functional NMDA receptors at axonal growth cones of young hippocampal neurons. *J Neurosci, 31*(25), 9289-9297. doi:10.1523/JNEUROSCI.5639-10.2011

Watanabe, M., Fukaya, M., Sakimura, K., Manabe, T., Mishina, M., & Inoue, Y. (1998). Selective scarcity of NMDA receptor channel subunits in the stratum lucidum (mossy fibre-recipient layer) of the mouse hippocampal CA3 subfield. *Eur J Neurosci, 10*(2), 478-487.

Wong, H. H., Rannio, S., Jones, V., Thomazeau, A., & Sjostrom, P. J. (2020). NMDA receptors in axons: there's no coincidence. *J Physiol*. doi:10.1113/JP280059

Woodhall, G., Evans, D. I., Cunningham, M. O., & Jones, R. S. (2001). NR2B-containing NMDA autoreceptors at synapses on entorhinal cortical neurons. *J Neurophysiol, 86*(4), 1644-1651. doi:10.1152/jn.2001.86.4.1644

Yan, Q., Rosenfeld, R. D., Matheson, C. R., Hawkins, N., Lopez, O. T., Bennett, L., & Welcher, A. A. (1997). Expression of brain-derived neurotrophic factor protein in the adult rat central nervous system. *Neuroscience, 78*(2), 431-448.

Yang, J., Woodhall, G. L., & Jones, R. S. (2006). Tonic facilitation of glutamate release by presynaptic NR2B-containing NMDA receptors is increased in the entorhinal cortex of chronically epileptic rats. *J Neurosci, 26*(2), 406-410. doi:10.1523/JNEUROSCI.4413-05.2006

Zeng, J., Thomson, L. M., Aicher, S. A., & Terman, G. W. (2006). Primary afferent NMDA receptors increase dorsal horn excitation and mediate opiate tolerance in neonatal rats. *J Neurosci, 26*(46), 12033-12042. doi:10.1523/JNEUROSCI.2530-06.2006

Zucca, S., Griguoli, M., Malezieux, M., Grosjean, N., Carta, M., & Mulle, C. (2017). Control of Spike Transfer at Hippocampal Mossy Fiber Synapses In Vivo by GABAA and GABAB Receptor-Mediated Inhibition. *J Neurosci, 37*(3), 587-598. doi:10.1523/JNEUROSCI.2057-16.2016

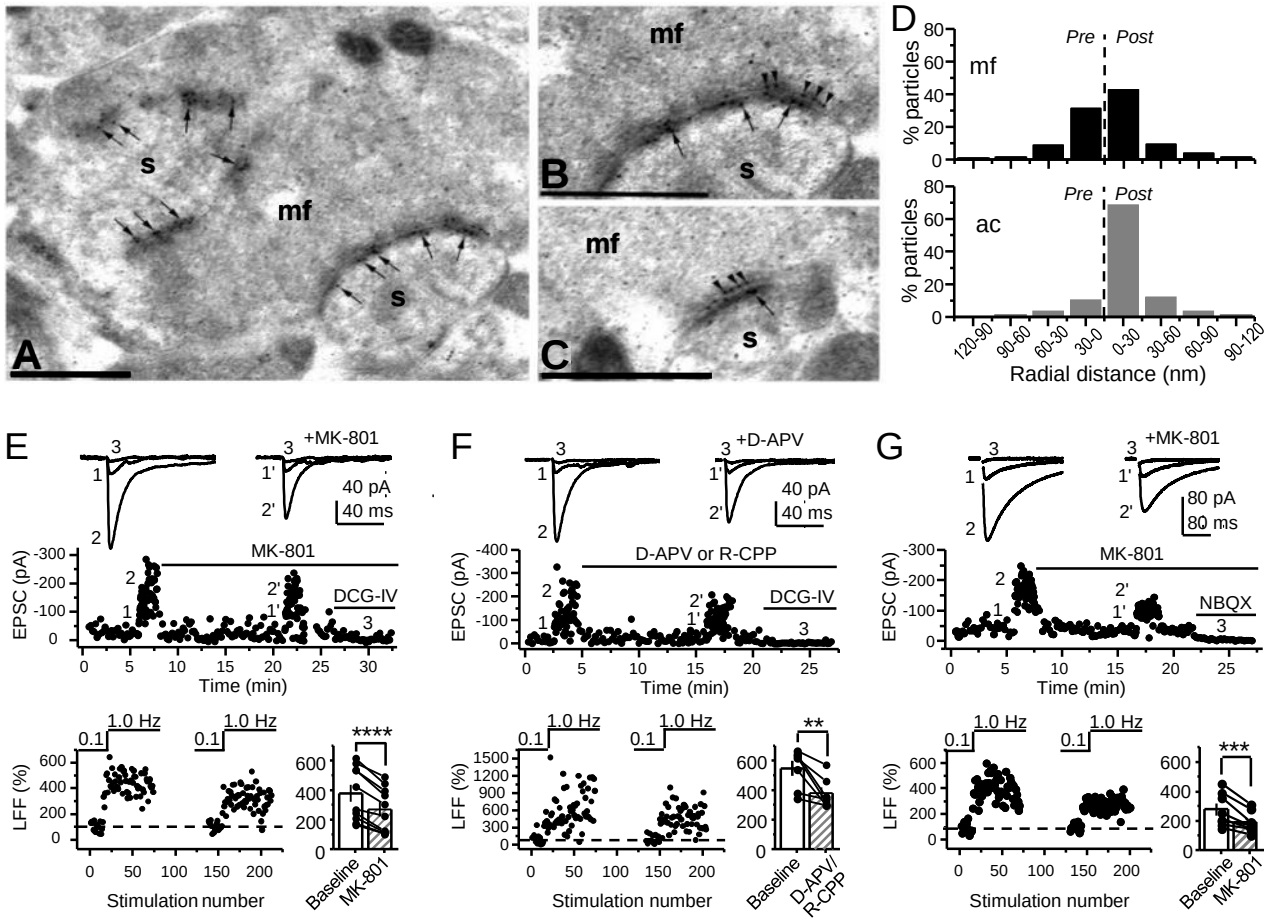

Figure 1. Anatomical and functional evidence for preNMDARs at mossy fiber synapses. (A) Image of a mossy fiber (mf) giant bouton and postsynaptic spines (s). **(B, C)** Higher magnification of mossy fiber synapses. Arrows indicate postsynaptic GluN1 whereas arrowheads indicate presynaptic GluN1. Calibration bars: 500 nm. **(D)** Mossy fiber (mf) and associational commissural (ac) synaptic GluN1 immuno-particle radial distribution (30 nm bins), mf: 34 synapses, 100 presynaptic particles; ac: 25 synapses, 24 presynaptic particles; 3 animals. **(E)** AMPAR-ESPCs were recorded at Vh= -70 mV in the presence of 0.5 µM LY303070 and 100 µM picrotoxin. Low-frequency facilitation (LFF), induced by stepping stimulation frequency from 0.1 to 1 Hz, was assessed before and after bath application of MK-801 (50 µM). MK-801 significantly reduced LFF (baseline 378 ± 57%, MK-801 270 ± 48%, n = 10 cells; baseline vs MK-801, $p = 3.8 \times 10^{-5}$, paired *t*-test). In all panels of this figure: representative traces (*top*), representative experiment (*middle*), normalized LFF and summary plot (*bottom*). DCG-IV (1 µM) was applied at the end of all recordings to confirm mf-CA3 transmission. **(F)** D-APV or R-CPP (50-100 µM) application also reduced LFF (baseline 546 ± 50%, D-APV/R-CPP 380 ± 38%, n = 7 cells; baseline vs D-APV/R-CPP, p = 0.00743, paired *t*-test). **(G)** KAR-EPSCs were recorded at Vh= -70 mV in the presence of 15 µM LY303070 and 100 µM picrotoxin. In addition, NMDAR-mediated transmission was blocked intracellularly by loading MK-801 (2 mM) in the patch-pipette. Bath application of MK-801 (50 µM) significantly reduced LFF (baseline 278 ± 40%, MK-801 195 ± 26% n = 8 cells; baseline vs MK-801, p = 0.00259, paired *t*-test). Data are presented as mean ± s.e.m. ** $p < 0.01$; *** < 0.005; **** $p < 0.001$.

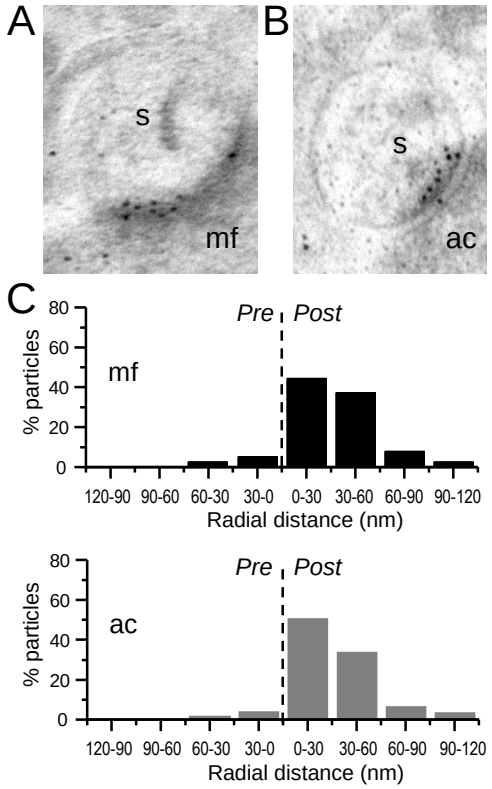

Supplementary Figure 1 related to Figure 1. Immunogold-EM reveals negligible presynaptic AMPAR particle distribution. **(A,B)** Images of mossy fiber (mf) and associational commissural (ac) synapses, postsynaptic spines (s). **(C)** AMPAR immuno-particle distribution (30 nm bins), mf: 102 synapses, 8 presynaptic particles; ac: 75 synapses, 6 presynaptic particles; 3 animals. Dashed line represents synaptic cleft.

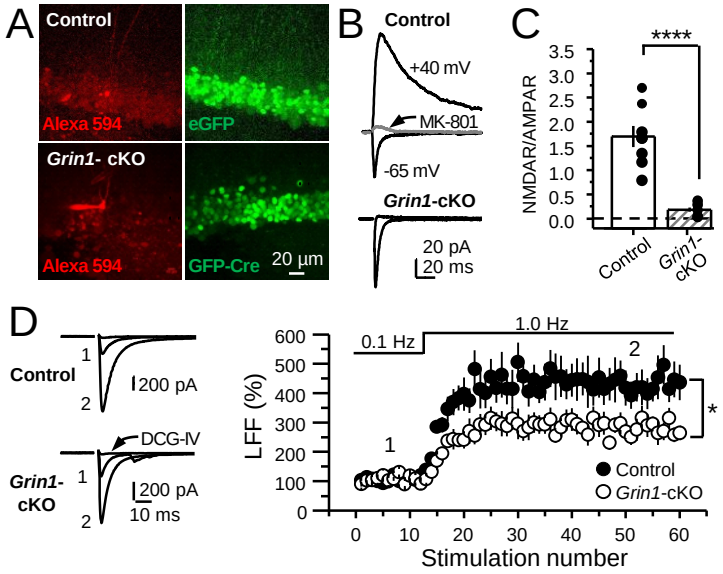

Figure 2. GluN1 deletion from granule cells reduces mf-CA3 facilitation. (A) Representative images showing GCs patch-loaded with Alexa 594 (35 µM) *(left),* and GFP expression in GCs *(right)*. **(B)** Representative EPSCs recorded from control (GFP$^+$) and *Grin1*-cKO (Cre-GFP$^+$) GCs. Synaptic responses were elicited by activating medial perforant-path inputs. AMPAR-ESPCs were recorded at Vh= -65 mV in the presence of 100 µM picrotoxin, NMDAR-EPSCs were isolated with 10 µM NBQX and recorded at +40 mV. MK-801 (20 µM) was applied at the end of each recording. **(C)** Summary plot demonstrating that GluN1 deletion from GCs virtually abolished NMDAR-mediated transmission indicated by a strong reduction of NMDAR/AMPAR in *Grin1*-cKO GCs as compared to controls (control 1.61 ± 0.18, n = 9 cells, *Grin1*-cKO 0.18 ± 0.04, n = 10 cells; control vs *Grin1*-cKO, $p = 9.2 \times 10^{-6}$, unpaired *t*-test). **(D)** LFF was significantly reduced in GluN1-deficient animals (control, 430 ± 5 %, n = 13 cells; *Grin1*-cKO, 291 ± 6 %, n = 11 cells; p = 0.0239, unpaired *t*-test). Representative traces (*left*) and summary plot (*right*). LFF was induced by stepping stimulation frequency from 0.1 to 1 Hz. DCG-IV (1 µM) was added at the end of each experiment. Data are presented as mean ± s.e.m. * $p < 0.05$; **** $p < 0.001$

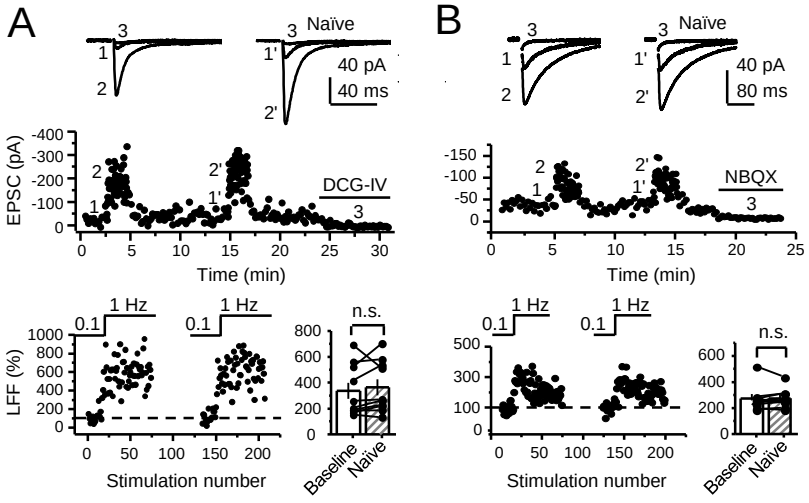

Supplementary Figure 2 related to Figure 1. (A) Stable low-frequency facilitation (LFF) of AMPAR-EPSCs. In naïve slices (interleaved experiments), LFF remained unchanged throughout the recording session (baseline 335 ± 62%, naïve 363 ± 63%, n = 10 cells, p = 0.185, Wilcoxon-Signed Ranks test baseline vs naïve). DCG-IV (1 µM) was applied at the end of all recordings to confirm mf-CA3 transmission. **(B)** LFF of KAR-EPSCs was also stable in interleaved, naïve slices (baseline 274 ± 33%, naïve 278 ± 25%, n = 9 cells; p = 0.236, Wilcoxon Signed Ranks test, baseline vs naïve). NBQX (10 µM) was applied at the end of all recordings to confirm mossy fiber KAR transmission. Data are presented as mean ± s.e.m.

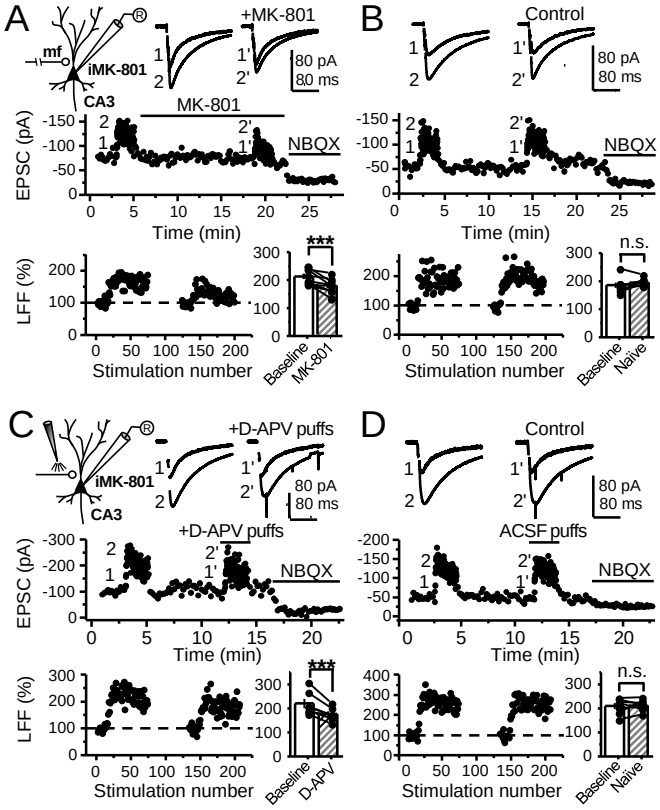

Figure 3. Reduced facilitation by NMDAR antagonism is independent of the GC somatodendritic compartment. (A) KAR-EPSCs were recorded at Vh= -70 mV in the presence of 15 µM LY303070 and 100 µM picrotoxin. In addition, NMDAR-mediated transmission was blocked intracellularly by loading MK-801 (2 mM) in the patch-pipette. LFF of KAR-EPSCs was assessed as in Fig. 1G but with transected mossy fiber axons (see Methods). Bath application of MK-801 (50 µM) significantly reduced LFF (baseline 213 ± 9%, MK-801 181 ± 10%, n = 8 cells; baseline vs MK-801, p = 0.002, paired *t*-test). In all panels of this figure: recording arrangement (*inset*), representative traces (*top*), representative experiment (*middle*), normalized LFF and summary plot (*bottom*). **(B)** Stable LFF in transected, naïve slices (baseline 186 ± 10%, naïve 196 ± 5%, n = 8 cells, baseline vs naïve, p = 0.278, paired *t*-test). **(C)** LFF was induced before and during puff application of D-APV (2 mM) in *stratum lucidum*. This manipulation significantly reduced facilitation (baseline 220 ± 19%, D-APV puff 176 ± 11%, n = 7 cells; baseline vs D-APV puff, p = 0.003, paired *t*-test). **(D)** Stable LFF in acute slices during puff application of ACSF (baseline 210% ± 12, naïve 213% ± 9, n = 7 cells; baseline vs naïve, p = 0.778, paired *t*-test). NBQX (10 µM) was applied at the end of all recordings to confirm mossy fiber KAR transmission. Data are presented as mean ± s.e.m. *** p < 0.005.

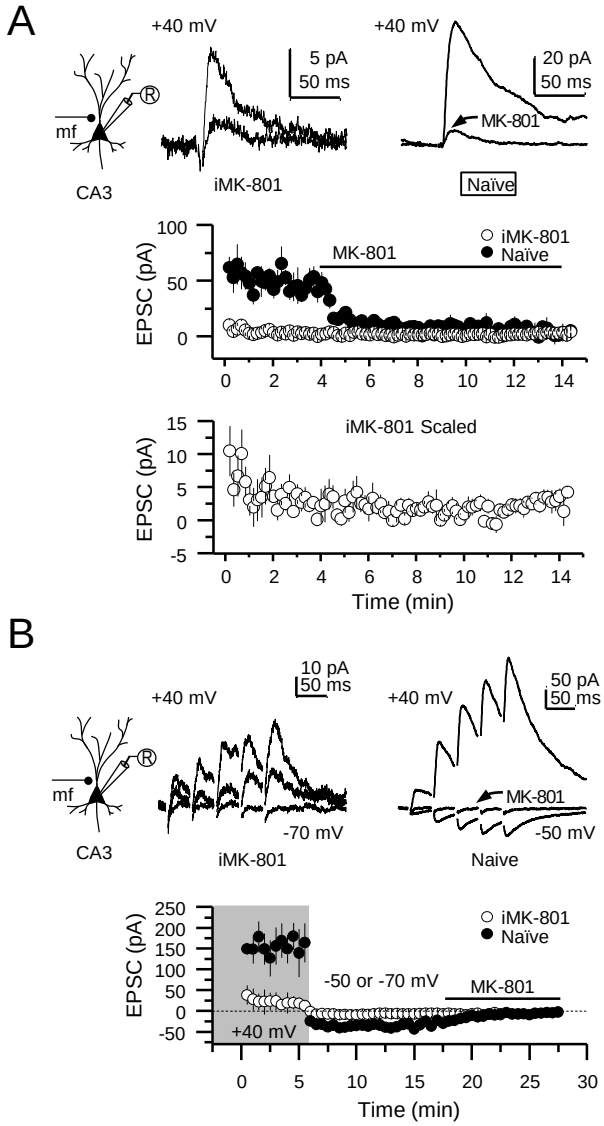

Supplementary Figure 3 related to Figures 1 & 4. Intracellular MK-801 effectively blocked postsynaptic NMDARs. In each panel of this figure, representative NMDAR-EPSCs from CA3 pyramidal neurons patch-loaded with 2 mM MK-801 *(left)* or naïve internal solution *(right)*. Mossy fiber inputs were stimulated with a bipolar electrode (theta-glass pipette) in *stratum lucidum* delivering 1 pulse or 5 pulses at 25 Hz in the presence of PTX (100 µM) and NBQX (10 µM). **(A)** NMDAR currents were recorded at Vh = + 40 mV in intracellular MK-801 (iMK-801) and naïve conditions. Bath-application of MK-801 (50 µM) blocked NMDAR currents in naïve cells to a similar magnitude as cells patch-loaded with MK-801 (n = 5 cells in each condition, U = 0.0122, Mann-Whitney test). Note that CA3 pyramidal neurons were loaded for at least 3-5 minutes before recording started at +40 mV. **(B)** NMDAR currents were recorded at Vh= + 40 mV *(gray shaded area)* followed by a voltage jump to -70 mV in iMK-801 conditions and -50 mV in naïve recordings. Bath-application of MK-801 (50 µM) blocked NMDAR currents of the 5th pulse to a similar magnitude as iMK-801 (n = 5 cells per condition, U = 0.008, Mann-Whitney test). Data are presented as mean ± s.e.m.

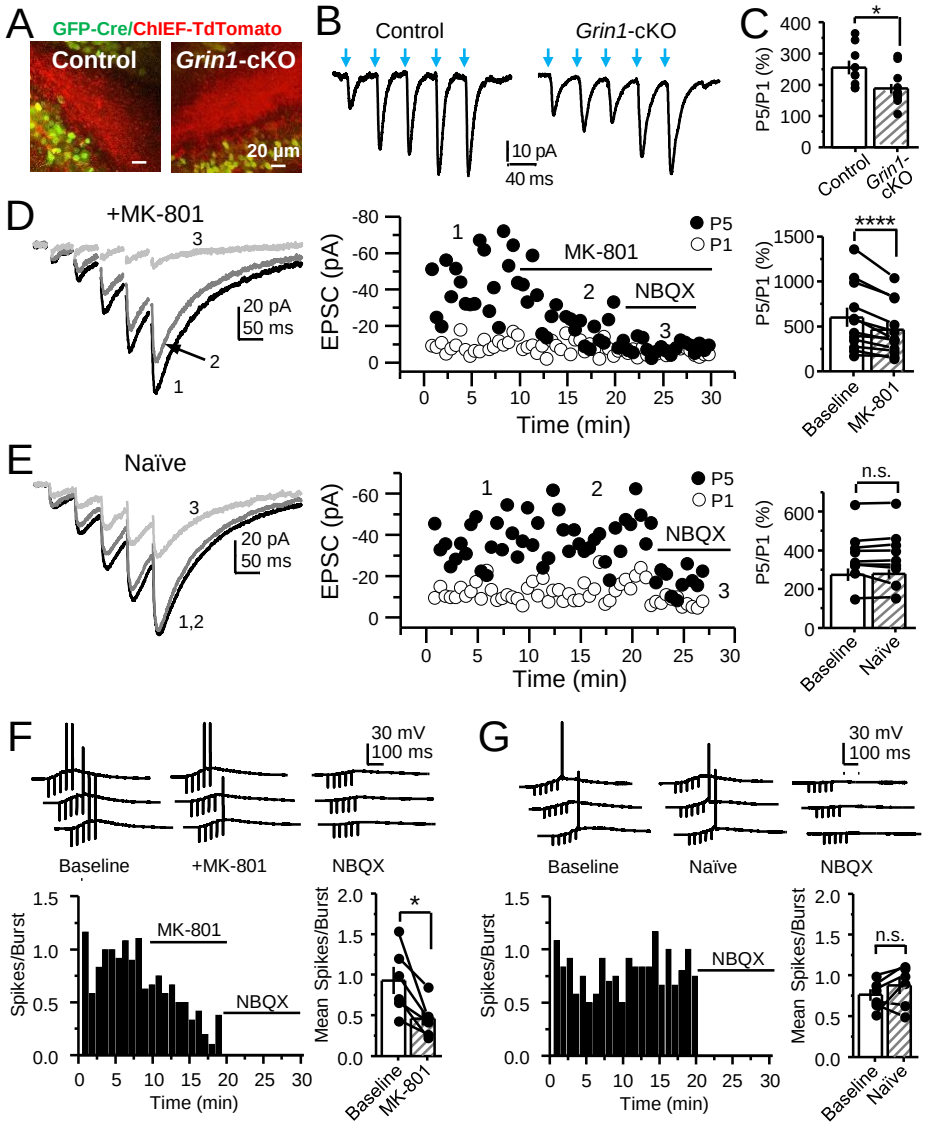

Figure 4. PreNMDARs contribute significantly to burst-induced facilitation and spike transfer. (A) Representative images showing expression of GFP-Cre *(left)* and ChiEF-tdTomato *(right)* in the DG of control and *Grin1*-cKO animals. **(B)** Representative AMPAR-EPSCs from control *(left)* and *Grin1*-cKO *(right)* CA3 pyramidal neurons recorded at Vh= -65 mV and evoked by optical burst-stimulation (5 pulses at 25 Hz) of *stratum lucidum*. Blue arrows indicate light stimulation. **(C)** Summary plot of burst-induced facilitation measured as P5/P1 ratio of optical responses; facilitation was significantly reduced in *Grin1*-cKO animals as compared to control (*Grin1*-cKO 187 ± 16%, n = 12 cells, control 255 ± 22%, n = 9 cells; *Grin1*-cKO vs control, p = 0.0167, unpaired *t*-test). **(D)** Burst-stimulation induced KAR-EPSCs that were isolated and recorded as described in Fig. 3, bath-application of MK-801 (50 µM) significantly reduced facilitation (baseline 601 ± 107%, MK-801 464 ± 84%, n = 13 cells; baseline vs MK-801, p = 0.00042, paired *t*-test). In panels D and E of this figure: representative traces (*left*), representative experiment (*middle*), and summary plot (*right*). **(E)** Burst-induced facilitation was stable in interleaved, naïve slices (baseline 369 ± 45%, naïve 367 ± 48%, n = 9 cells, p = 0.863, paired *t*-test). **(F)** Bath-application of MK-801 (50 µM) reduced KAR-mediated action potentials induced by burst-stimulation (baseline 0.93 ± 0.17, MK-801 0.46 ± 0.09, n = 6 cells, p = 0.036, Wilcoxon Signed Ranks test). In panels F and G of this figure: representative traces (*top)*, representative experiment and summary plot (*bottom)*. **(G)** Stable KAR-mediated action potentials in interleaved naïve slices (baseline 0.76 ± 0.07, naïve 0.88 ± 0.1, n = 6 cells, p = 0.2084, Wilcoxon Signed Ranks test). NBQX (10 µM) was applied at the end of all experiments in panels D-G. Data are presented as mean ± s.e.m. * p < 0.05; **** p < 0.001

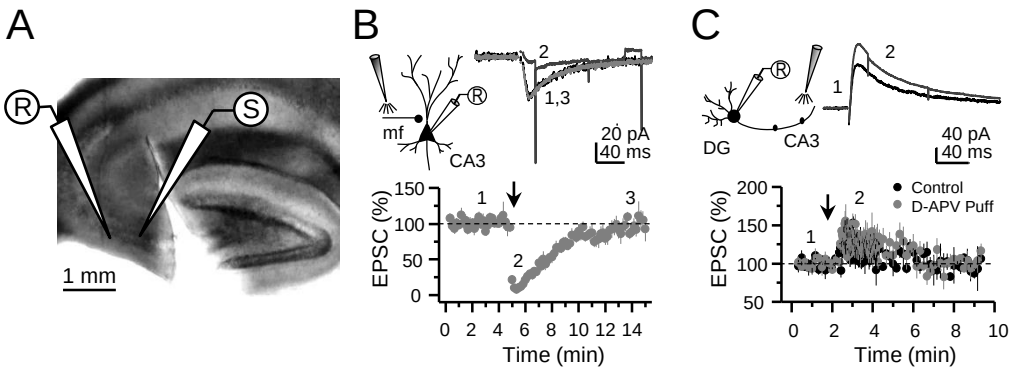

Supplementary Figure 4 related to Figure 3. Targeting preNMDARs in mf axons but not granule cells. **(A)** Field view of a representative hippocampal slice showing a surgical cut between DG and CA3. **(B)** Local D-APV puff application (vertical arrow, 2 puffs at 0.1 Hz) blocks NMDAR currents recorded at Vh= -50 mV and washes out in less than 10 minutes (n = 7 cells, p = 5 x 10^{-8}, paired *t*-test). Inset depicts the recording paradigm of the experiment *(left)*, the representative NMDAR currents *(top)* and the summary time course *(bottom)* where arrows denote the onset of D-APV (2 mM) puff application. Mossy fiber were stimulated with a bipolar electrode (theta-glass pipette) in *stratum lucidum* in the presence of 100 µM PTX and 10 µM NBQX. **(C)** D-APV puff application in CA3 did not reduce NMDAR transmission in GCs (n = 6 cells, control vs D-APV puff, U = 0.594, Mann Whitney test). Excitatory inputs were stimulated with a monopolar electrode placed in the medial molecular layer, in the presence of 100 µM PTX and 10 µM NBQX, and while GCs were clamped at Vh= +40 mV. Data are presented as mean ± s.e.m.

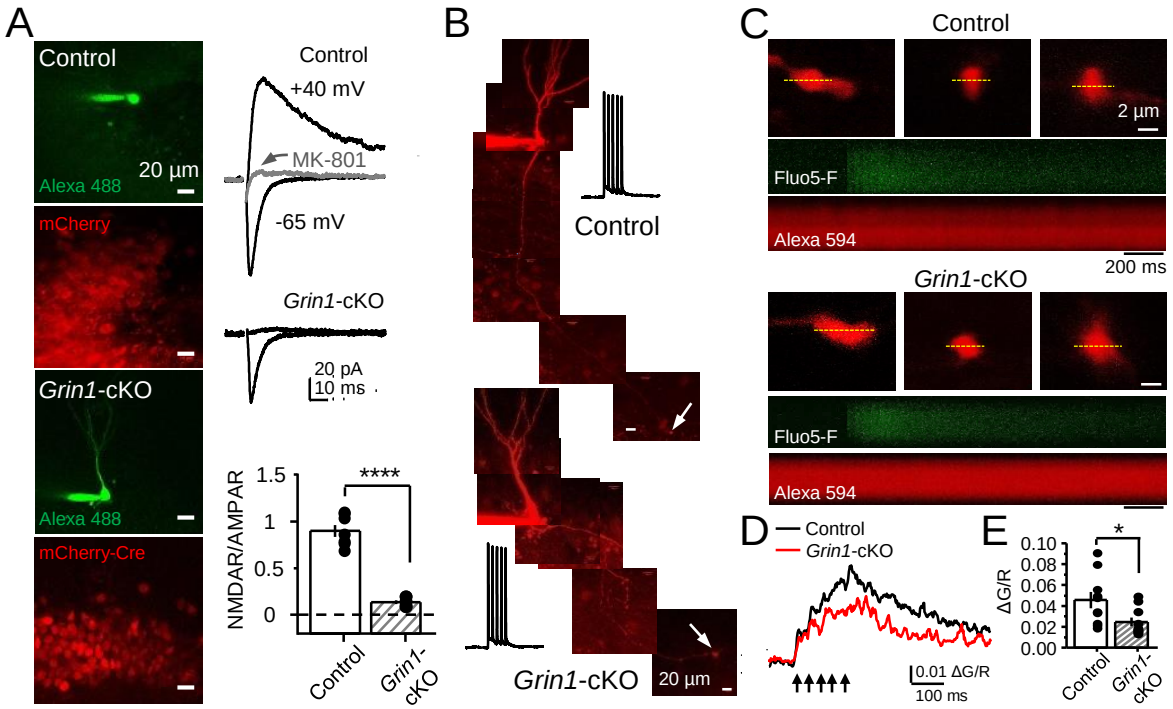

Figure 5. preNMDARs contribute to presynaptic Ca^{2+} rise. (A) Representative images showing GCs patch-loaded with Alexa 488 (35 µM) to confirm expression of mCherry *(bottom)*. Representative EPSCs recorded from control *(top)* or *Grin1*-cKO *(middle)* GCs. Synaptic responses were elicited by activating medial perforant-path inputs. AMPAR-ESPCs were recorded at Vh= -65 mV in the presence of 100 µM PTX, NMDAR-EPSCs were isolated with 10 µM NBQX and recorded at +40 mV. MK-801 (20 µM) was applied at the end of each experiment. Summary plot *(bottom)* demonstrating that GluN1 deletion from granule cells virtually abolished NMDAR-mediated transmission indicated by a strong reduction of NMDAR/AMPAR in *Grin1*-cKO granule cells as compared to controls (control 0.90 ± 0.17, n = 7 cells, *Grin1*-cKO 0.13 ± 0.05, n = 6 cells; control vs *Grin1*-cKO, $p = 3.81 \times 10^{-7}$, unpaired *t*-test). **(B)** Representative control and *Grin1*-cKO granule cells patch-loaded with Fluo-5F (200 µM) and Alexa 594 (35 µM). Arrows indicate the identification of a mossy fiber giant bouton. **(C)** Three representative mossy fiber boutons *(top)* and line scan analysis of calcium transients (CaTs) elicited by action potential stimulation of 5 APs at 25 Hz *(bottom)*, in Control and *Grin1*-cKO animals. Dotted line (yellow) indicates line scan. Red Channel, Alexa 594; Green Channel, Fluo5-F. **(D, E)** Peak analysis of the 5^{th} pulse ΔG/R revealed a significant reduction in calcium rise of *Grin1*-cKO animals as compared to Control (control 0.046 ± 0.01, n = 10 boutons, *Grin1*-cKO 0.025 ± 0.004, n = 10 boutons; control vs. *Grin1*-cKO, U = 0.017, Mann-Whitney test). Arrows indicate mossy fiber activation. Data are presented as mean ± s.e.m. * U < 0.05; **** p < 0.001

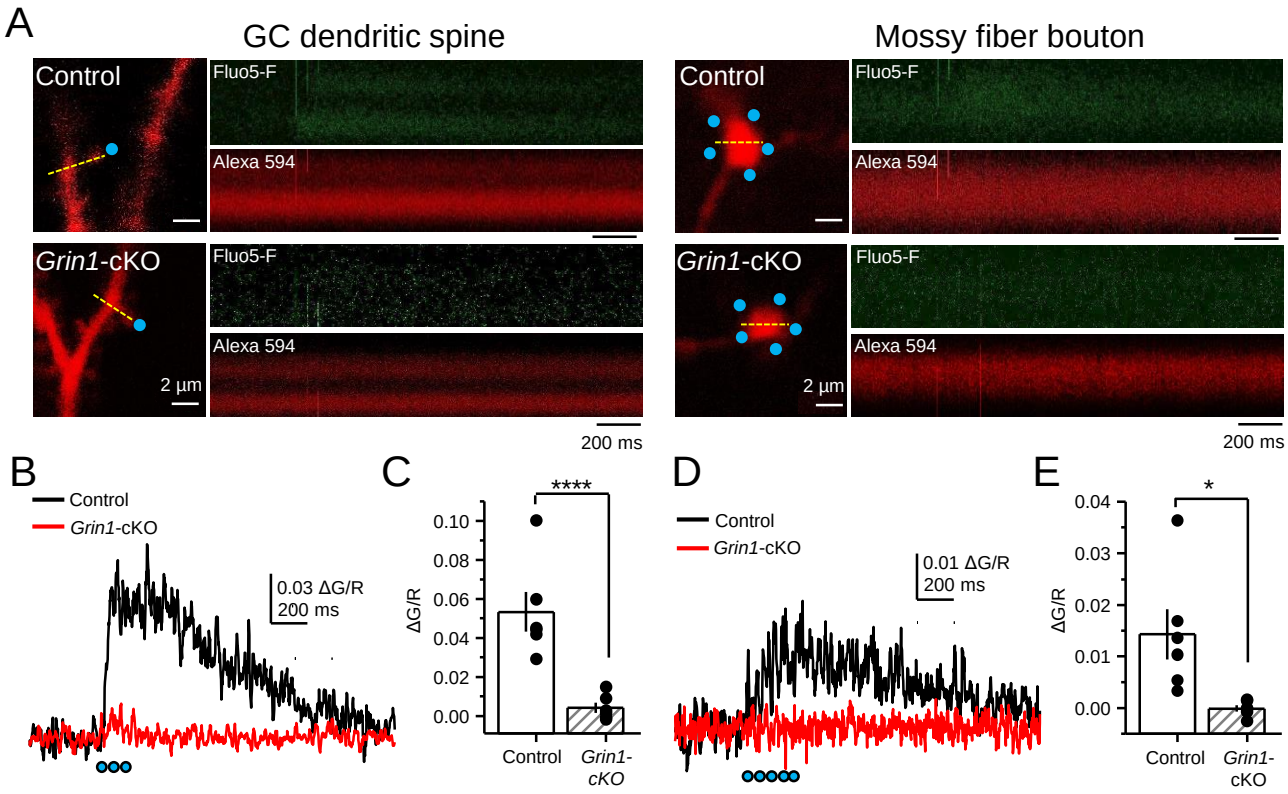

Figure 6. Uncaging glutamate induces Ca^{2+} rise mossy fiber boutons. (A) Representative images showing dendritic spines in GCs *(left)* and mossy fiber boutons *(right),* and the associated line scan analysis of calcium transients (CaTs) elicited by uncaging of MNI-glutamate (see Methods), in control and *Grin1*-cKO animals. Blue dots indicate uncaging spots. Red Channel, Alexa 594; Green Channel, Fluo5-F. **(B)** Line scan analysis of CaTs measuring ΔG/R in dendritic spines when MNI-glutamate is uncaged in control or *Grin1*-cKO animals. Blue dots indicate 2PU pulses. **(C)** Summary plot demonstrating a significant reduction in dendritic spine CaTs in *Grin1*-cKO as compared to Control (control 0.053 ± 0.01 ΔG/R, n = 6 dendritic spines, *Grin1*-cKO 0.004 ± 0.003 ΔG/R, n = 6 spines; ΔG/R control vs. *Grin1*-cKO, p = 0.00088, unpaired *t*-test). **(D)** Line scan analysis of CaTs measuring ΔG/R in mossy fiber boutons when MNI-glutamate is uncaged in control or *Grin1*-cKO animals. **(E)** Summary plot demonstrating significant CaTs in boutons of control as compared to *Grin1*-cKO (control 0.014 ± 0.005, n = 6 boutons, *Grin1*-cKO -0.00012 ± -0.0006, n = 6 boutons; control vs. *Grin1*-cKO, p = 0.015, unpaired *t*-test). Data are presented as mean ± s.e.m. * p < 0.05; **** p < 0.001.

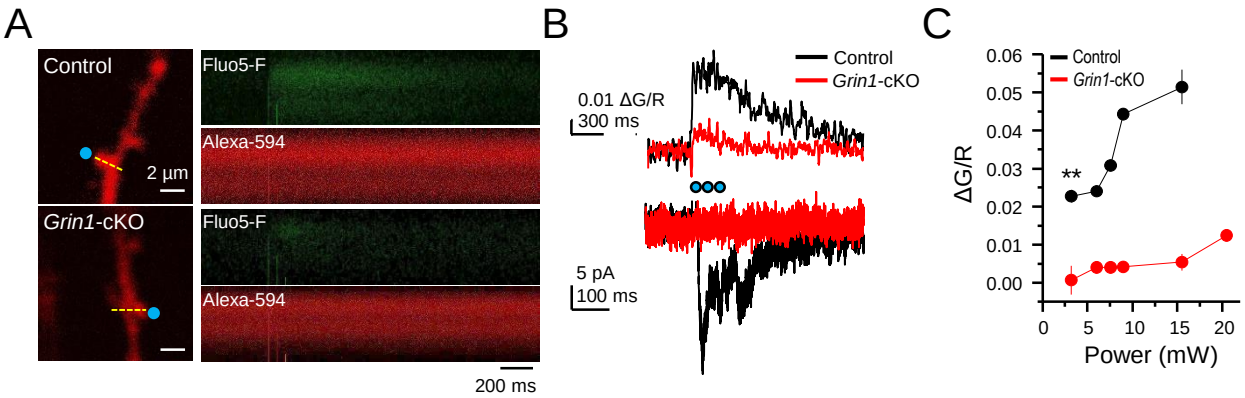

Supplementary Figure 5 related to Figure 6. *Grin1*-cKO exhibit reduced CaTs at varying uncaging laser power intensities**. (A)** Representative images of CaTs from control *(top)* and G*rin1*-cKO animals *(bottom)* after MNI-glutamate uncaging (2 mM, 3 pulses at 25 Hz) on GC dendritic spines. Dotted line (yellow) indicates line scan, and blue dots indicate uncaging spots. **(B)** Quantified ΔG/R signals *(top)* and uncaging induced NMDAR-EPSCs *(bottom)* from control and *Grin1*-cKO animals. Blue dots indicate 2PU pulses **(C)** Control animals display robust ΔG/R signals as compared to *Grin1*-cKO animals at varying laser power intensities (6 spines per group, U = 0.00507 per power intensity, Mann-Whitney test). Data are presented as mean ± s.e.m. ** U < 0.01.

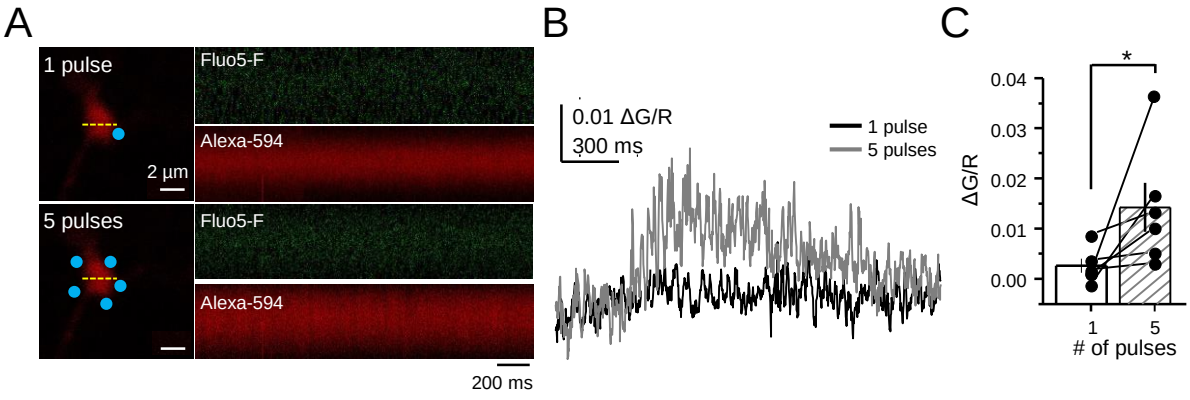

Supplementary Figure 6 related to Figure 6. Bouton CaTs can be detected after repetitive uncaging of MNI-glutamate. **(A)** Representative images of CaTs from single-trial: 1 pulse *(top)* and 5 pulses, 25 Hz *(bottom)* of MNI-glutamate uncaging (2 mM). Dotted line (yellow) indicates line scan, and blue dots indicate uncaging spots. **(B)** Quantified ΔG/R signals from 1 pulse *(black)* and 5 pulses *(dark gray)* from all trials. **(C)** Repetitive pulses display robust ΔG/R signals as compared to single pulses (n = 6 boutons, p = 0.03603, Wilcoxon-Signed Ranks test). Data are presented as mean ± s.e.m. * $p < 0.05$.

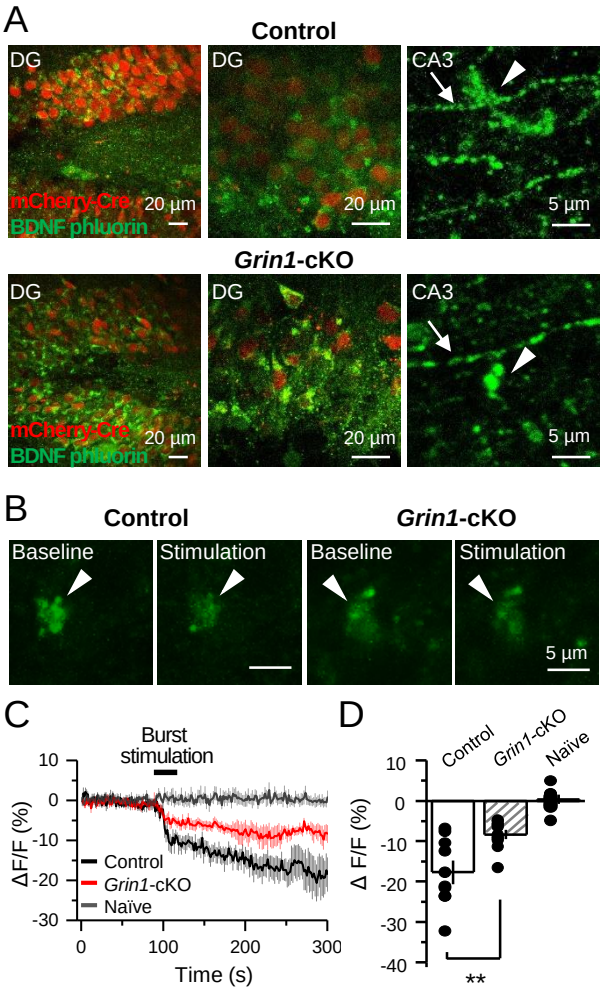

Figure 7. preNMDARs contribute significantly to BDNF release following repetitive activity. (A) Representative images showing expression of BDNF-pHluorin in the DG and CA3 area (arrows indicate mossy fiber axon, arrowheads indicate mossy fiber boutons). Control images *(top)*, *Grin1*-cKO images *(bottom)*. **(B)** Representative images of BDNF-pHluorin signal intensity at baseline and after repetitive stimulation of mossy fibers (125 pulses, 25 Hz, x 2). Control images *(left)*, *Grin1*-cKO images *(right*), arrowhead indicates region of interest. **(C)** Time course of BDNF-pHluorin signal intensity measured as ΔF/F (%): control *(black)*, *Grin1*-cKO *(red),* Naïve *(gray)*. **(D)** Quantification of BDNF-pHluorin signal in (C) during the last 100 seconds reveals larger BDNF release in control animals as compared to *Grin1*-cKO (control -18% ± 3%, n = 12 slices, *Grin1*-cKO -8 ± 1%, n = 10 slices, *Grin1*-cKO vs. control, p = 0.00648, unpaired *t*-test). Data are presented as mean ± s.e.m. ** p < 0.01.

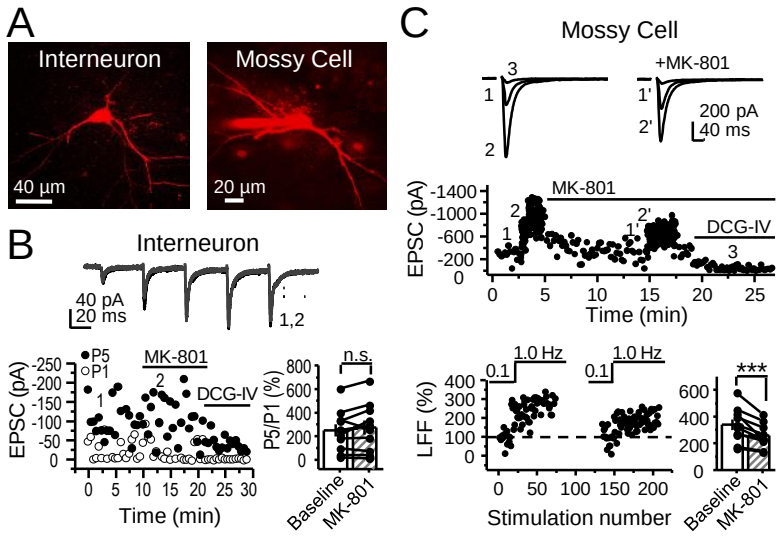

Figure 8. preNMDARs contribute to synaptic facilitation of mossy fiber inputs onto mossy cells but not inhibitory interneurons. (A) Representative images showing a CA3 interneuron and a hilar mossy cell patch-loaded with Alexa 594 (35 µM) for morphological identification in acute slices. **(B)** AMPAR-EPSCs were recorded from CA3 interneurons at Vh= -65 mV and burst-stimulation was elicited by 5 pulses at 25 Hz, see traces *(top)*. Representative experiment *(bottom, left)*, and summary plot *(bottom, right)* showing bath-application of MK-801 (50 µM) had no significant effect on facilitation measured by P5/P1 ratio (Baseline: 248 ± 51%; MK-801: 275 ± 60%, n = 11, MK-801 vs baseline, p = 0.1411, paired *t*-test). **(C)** AMPAR-ESPCs were recorded at Vh = -70 mV from hilar mossy cells, LFF was induced by stepping stimulation frequency from 0.1 to 1 Hz, see traces *(top)*. Representative experiment *(middle)*, normalized LFF and summary plot *(bottom)* indicating bath-application of MK-801 (50 µM) reduced facilitation (baseline 350 ± 10%, MK-801 225 ± 25%, n = 9 cells; baseline vs MK-801, p = 0.00152, paired *t*-test). DCG-IV (1 µM) was applied at the end of all experiments. Data are presented as mean ± s.e.m. *** $p < 0.005$.

Figure	Normality Test (Shapiro-Wilk)	Test used	N	P value
1D			3 animals	
1E	passed	paired *t*-test	10 cells	$p < 0.001$ $p = 0.000038$
1F	passed	paired *t*-test	7 cells	$p < 0.01$ $p = 0.00743$
1G	passed	paired *t*-test	8 cells	$p < 0.005$ $p = 0.00259$
S1C			3 animals	
2C	Control: passed *Grin1*-cKO: passed	unpaired *t*-test	Control: 9 cells *Grin1*-cKO: 10 cells	$p < 0.001$ $p = 0.0000092$
2D	Control: passed *Grin1*-cKO: passed	unpaired *t*-test	Control: 13 cells *Grin1*-cKO: 11 cells	$p < 0.05$ $p = 0.0239$
S2A	rejected	Wilcoxon Signed Ranks test	10 cells	$p > 0.1$ $p = 0.185$
S2B	rejected	Wilcoxon Signed Ranks test	9 cells	$p > 0.1$ $p = 0.236$
3A	passed	paired *t*-test	8 cells	$p < 0.005$ $p = 0.002$
3B	passed	paired *t*-test	8 cells	$p > 0.1$ $p = 0.278$
3C	passed	paired *t*-test	7 cells	$p < 0.005$ $p = 0.003$
3D	passed	paired *t*-test	7 cells	$p > 0.1$ $p = 0.778$
S3A	Naïve: passed iMK-801: passed	Mann-Whitney test	Naïve: 5 cells iMK-801: 5 cells	$U = 0.0122$
S3B	Naïve: passed iMK-801: passed	Mann-Whitney test	Naïve: 5 cells iMK-801: 5 cells	$U = 0.008$
4C	Control: passed *Grink1*-cKO: passed	unpaired *t*-test	Control: 9 cells *Grin1*-cKO: 12 cells	$p < 0.05$ $p = 0.0167$
4D	passed	paired *t*-test	13 cells	$p < 0.001$ $p = 0.00042$
4E	passed	paired *t*-test	9 cells	$p > 0.5$ $p = 0.863$
4F	passed	Wilcoxon Signed Ranks test	6 cells	$p < 0.05$ $p = 0.036$
4G	passed	Wilcoxon Signed Ranks test	6 cells	$p > 0.2$ $p = 0.2084$
S4B	passed	paired *t*-test	7 cells	$p < 0.001$ $p = 0.00000005$
S4C	passed	Mann-Whitney test	6 cells	$U = 0.594$
5A	Control: passed *Grin1*-cKO: passed	unpaired *t*-test	Control: 7 cells *Grin1*-cKO: 6 cells	$p < 0.001$ $p = 0.000000381$
5E	Control: passed *Grin1*-cKO: rejected	Mann-Whitney test	Control: 10 boutons *Grin1*-cKO: 10 boutons	$U = 0.017$
6C	Control: passed *Grin1*-cKO: passed	unpaired *t*-test	Control: 6 spines *Grin1*-cKO: 6 spines	$p < 0.001$ $p = 0.00088$

6E	Control: passed *Grin1*-cKO: passed	unpaired *t*-test	Control: 6 boutons *Grin1*-cKO: 6 boutons	$p < 0.05$ $p = 0.015$
S5C	Control: passed *Grin1*-cKO: rejected	Mann-Whitney test	Control: 6 spines *Grin1*-cKO: 6 spines	U = 0.00507
S6C	1 pulse: passed 5 pulses: passed	Wilcoxon Signed Ranks test	1 pulse: 6 boutons 5 pulses: 6 boutons	$p < 0.05$ $p = 0.03603$
7D	Control: passed *Grin1*-cKO: passed	unpaired *t*-test	Control: 12 slices *Grin1*-cKO: 10 slices	$p < 0.01$ $p = 0.00648$
8B	passed	paired *t*-test	11 cells	$p > 0.1$ $p = 0.1411$
8C	passed	paired *t*-test	10 cells	$p < 0.005$ $p = 0.00152$